TECTONICS, VOL. 19, NO. 6, PAGES 1065-1094 DECEMBER 2000

Collision tectonics in the Swiss Alps: Insight from geodynamic modeling

O.A. Pfiffner and S. Ellis[1]
Geologisches Institut, Universität Bern, Bern, Switzerland

C. Beaumont
Oceanography Department, Dalhousie University, Halifax, Nova Scotia, Canada

Abstract. This paper compares results from two-dimensional finite element dynamic modeling with the kinematic evolution of the Swiss Alps during the collision phase. In particular, we investigate the role of inherited lateral strength heterogeneities on orogenesis. A number of first-order characteristics are directly comparable at crustal scales. In the models the entry of continental crust into the convergent margin marks the end of near-perfect subduction. Accretion of material of the subducting plate to the upper plate creates an orogenic wedge on the incoming (pro)side and initiates a retroshear zone (or model backthrust). The addition of material to the upper plate builds a bivergent orogen. Heterogeneities in the pro-crust focus shear and lead to the development of "nappe structures" The combined action of pro-shear (nappe stacking) and retroshear (backthrusting) uplifts a plug between the two shear zones. Subsequent focusing of shear along the retroshear zone results in rotation of the plug and overlying units, leading to crustal-scale backfolds as observed in the Swiss Alps. The model experiments predict features relevant to Alpine dynamics, including (1) similar crustal thicknesses and exhumation patterns to those observed in the Swiss Alps today for erosion rates comparable to natural ones (1 mm yr^{-1}), (2) continued accretion and subduction of upper crustal fragments allowing high-pressure metamorphic conditions, (3) tilting and exhumation of lower crust when a midcrustal weak zone is present, and (4) "shunting" of material across the strong lower crustal wedge of the upper plate.

1. Introduction

The Swiss Alps are a well-studied example of a change from subduction to collision during the terminal phases of a Wilson cycle. The results of recent projects, which included geophysical investigations, have provided insight into the deep structure of the Alps (see overview in section 4). These investigations highlighted the crustal structure in a transect through eastern Switzerland. Here the Alps are a bivergent orogen, in which upper crustal units were stacked northward and southward above an asymmetric subduction geometry involving lithospheric mantle and lower continental crust (Figures 1 and 2). In the core of the orogen, underplating of upper crustal units and subsequent exhumation exposed high-grade rocks at the surface.

The transect through eastern Switzerland has the advantage of a combined coverage of refraction and reflection seismic surveys. Axial plunges of up to 35° in this transect display a section of 30 km thickness through the crust (Figure 2) which has been intensively studied from the point of view of structural geology, metamorphic petrology, etc. Thus the structure and the evolution in time of this transect through the Alpine orogen is exceptionally well known.

The dynamics of small collisional orogens have previously been investigated using forward modeling techniques with some success (e.g. analog models [*Malavieille* 1984; *Shemenda and Grocholsky,* 1992], thermal-kinematic models [*Okaya et al.*, 1996; *Bousquet et al.*, 1997], critical wedge theory [*Platt,* 1986], and dynamic models [*Beaumont et al.*, 1996]). Those models which apply force or velocity boundary conditions representing far-field dynamics and solve for displacement with time (dynamic models) are useful to investigate first-order controls on deformation styles in cases such as the Alps. In this study, we extend earlier papers dealing with aspects of subduction-accretion dynamics [*Beaumont et al.*, 1999; *Ellis et al*, 1999] and the transition to collision [*Beaumont et al.*, 1996] to investigate the role that inherited material heterogeneities play during collision. We use the results from numerical model experiments to make inferences concerning the controls on Alpine evolution.

The aim is to understand some of the first-order characteristics typical for collisional orogens and particularly well documented for the Swiss Alps (Figure 2). These include the formation of the crustal root, the exhumation pattern, the bivergent nature of the orogen with the steep zone of backthrusting, the formation of an upper crustal nappe pile beneath a passively rotating oceanic suture, and the exhumation of a lower crustal section in the retropart of the orogen.

Our numerical models do not include all the complexities of a typical collisional orogen. In particular, questions of along-strike displacements, thermal evolution, strain softening and flexural loading in response to sedimentation in foreland basins are not addressed.

2. Numerical Model Experiments

A two-dimensional finite element numerical model is used to investigate deformation of crust and upper mantle

[1]Now at Institute of Geological and Nucelar Sciences, Lower Hutt, New Zealand

Paper number 2000TC900019.
0278-7407/00/2000TC900019$12.00

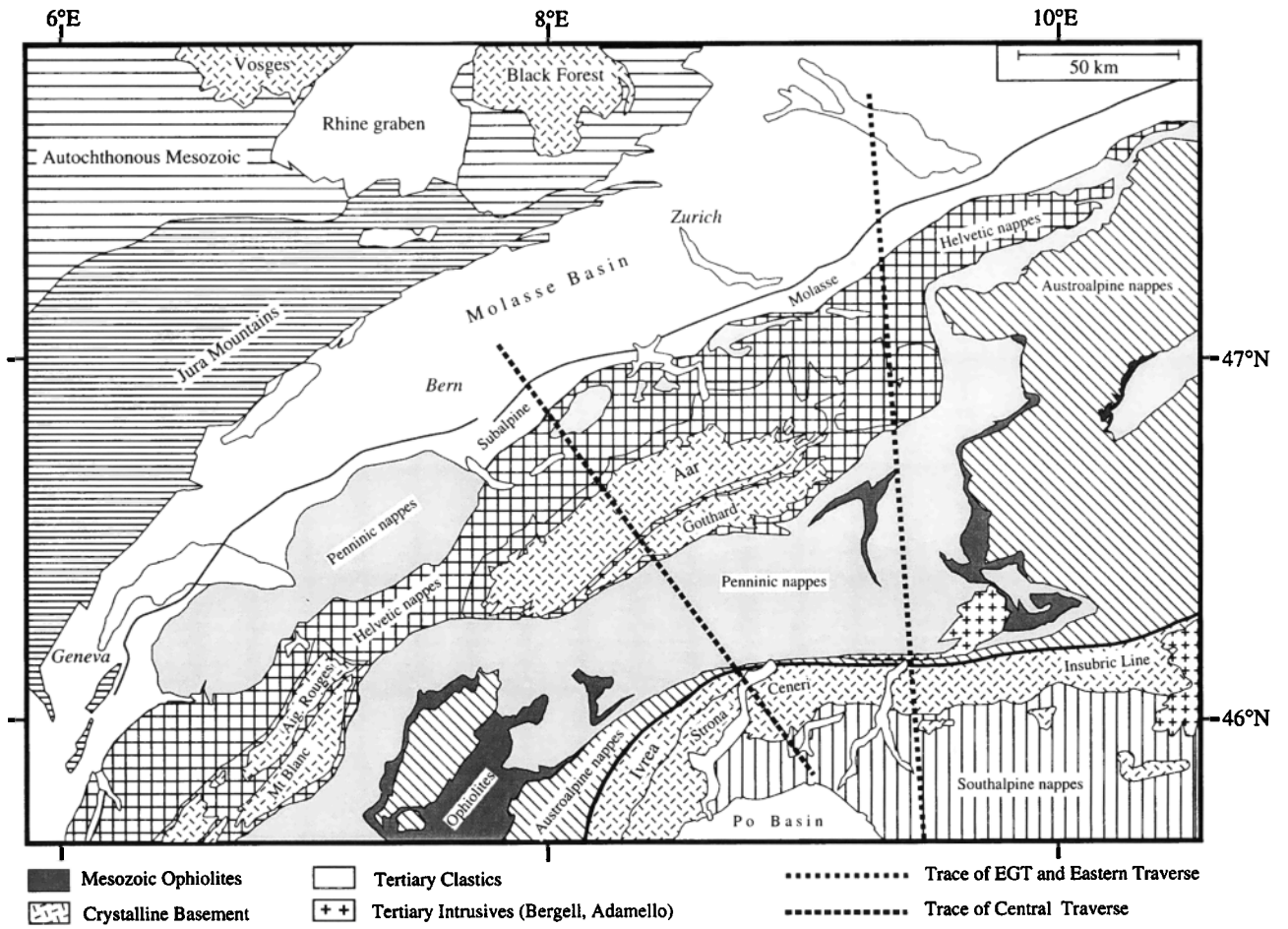

Figure 1. Tectonic map of the Swiss Alps showing major tectonic units and traces of transects pertaining to this study.

lithosphere in vertical cross sections, in response to boundary conditions representing subduction and collision (Figure 3) [*Fullsack*, 1995]. Only the top 60 km of the lithosphere is modeled. Behavior of lower lithosphere is represented by a velocity boundary condition on the base of the model domain. The dynamic model deforms under either Coulomb (frictional plastic) or thermally activated (viscous) power law creep, depending on whether the state of stress is on or below frictional yield stress. Thickening or thinning of the model lithosphere causes flexural isostatic adjustment and erosion at a rate depending on current height above baselevel. More details of the numerical model are given in Figure 3's caption and in the preceding papers investigating subduction dynamics [*Beaumont et al.*, 1999; *Ellis et al.*, 1999]. Here we describe the justification for the geometry and material properties used in the model and some of its limitations.

2.1. Model Geometry and Startup Phase

Subduction of oceanic crust and sediment is modeled in an initial phase prior to collision (Figure 3). Following *Willett et al.* [1993], the terms "pro" and "retro" are used to describe subduction geometry, where "proward" refers to direction toward the incoming plate and "retroward" refers to the opposite direction. We model oceanic sediment as a frictionally weak uniform layer, which becomes accreted at the interface between upper and lower plates during the initial subduction phase. The initial width of the model ocean and the relative flux balance between incoming and subducting material control the amount and thickness of material that is accreted at the suture. In all cases investigated here, this condition is set so that sediment underplates the margin prior to collision, corresponding to the near-Pure Subduction mode of *Beaumont et al.* [1999]. Model sediment is thicker (5 km thick) than at most real subduction margins, so that the accretion process is exaggerated, but subduction-accretion results for more realistic sediment thicknesses are qualitatively similar [cf. *Beaumont et al.*, 1999, Figures 6 and 7]. After accretion, we refer to this material as "suture material" during the collision phase. Note that the model rocks have no evolution in material properties or temperature, so that accreted suture material maintains the same frictional and viscous strength parameters throughout each model run, although the strength of frictional materials increases with pressure and therefore depth of burial. This approach is

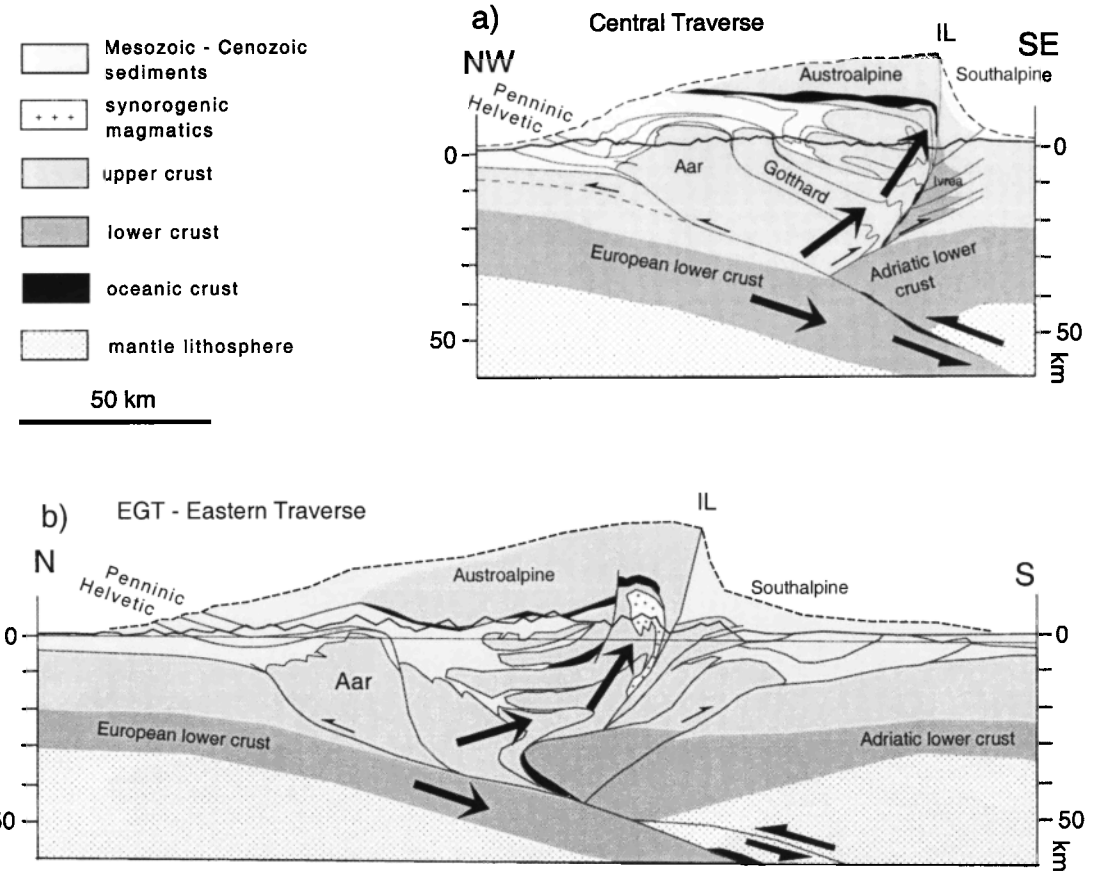

Figure 2. Two crustal-scale geological cross sections through the Swiss Alps based on seismic and structural data. For both transects a restored "eroded section" based on the estimated volume of eroded material is given. Transect traces are shown in Figure 1. The European lower crust and lithospheric mantle dip south beneath the Adriatic lower crust and mantle. (a) Central traverse [after *Pfiffner and Heitzmann*, 1997], which shows uplifted Adriatic lower crust to the south of the Insubric Line (IL). (b) Eastern traverse [after *Pfiffner and Hitz*, 1997; *Schmid et al.*, 1997a, 1997b] showing bivergent nature of the Alpine orogen at the upper crustal level.

obviously a simplification compared to Alpine-type orogens, where rocks are heated and metamorphosed upon burial.

2.2. Strength of Material Layers in the Crust and Mantle Lithosphere

Rock strength parameters based on the fit of empirical laws to laboratory experiments can be used to determine the transition between frictional and ductile behavior for a given material composition. These results have often been used in geodynamical models. However, there are problems with extrapolating laboratory data to geological strain rates [*Paterson*, 1987; *Carter and Tsenn*, 1987] and in determining appropriate flow laws for lower crustal rocks, particularly because only limited experimental studies of the strength of a major lower crustal constituent (feldspar) have been carried out [*Shelton and Tullis*, 1981; *Boland and Tullis*, 1986]. Using these experimental flow data, for average continental geothermal gradients (20°C km^{-1}) and geologically reasonable compressional strain rates the behavior of the lower crust is predicted to be ductile [e.g. *Ranalli and Murphy* , 1987; *Carter and Tsenn* , 1987; *Ord and Hobbs*, 1989]. In the case of the Alps, however, widespread ductile flow of the lower crust under equivalent conditions is not supported by current geophysical evidence [e.g. *Pfiffner and Hitz*, 1997; *Schmid et al.*, 1997a, 1997b; *Schmid*, 1999]. This suggests that the ductile flow laws based on rock experiments from hydrous single-phase minerals with intermediate compositions such as "wet" feldspar may underestimate the bulk strength of the lower crust, or that some process may cause strain localization and partitioning [*Axen et al.*, 1998; *Ellis et al.*, 1999].

Given the uncertainties in representing lower crustal flow laws, we have taken the simplest approach possible. Consistent with current observations that Alpine lower crust did not experience widespread detachment during deformation, we use a stronger set of material parameters than suggested by experimental flow law data so that lower crust remains in the frictional domain. In addition, for the first few experiments, we investigate the effect of the weak suture on subduction-collision transition for a uniformly strong, frictional crust (Table 1, E1-E4), which we regard as a limiting "strong" model. This allows us to isolate and investigate some of the dynamics involved in interaction between weak suture material

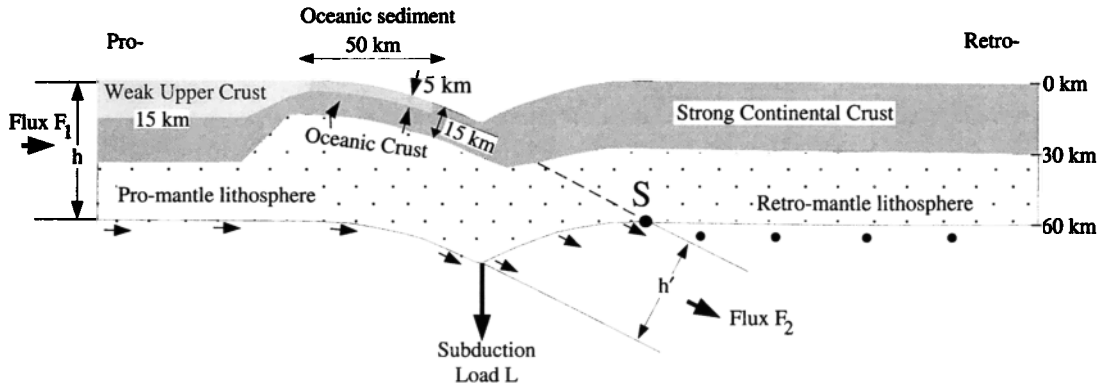

Layer	Internal Angle of Friction (ϕ)	Ductile Parameters
Oceanic sediment	Uniform 9°	n/a
Oceanic or Strong Continental Crust	Uniform 15°	"wet" feldspar[1] × 10
Weak Upper Crust	Uniform 15°	"wet" quartz[2]
Promantle Lithosphere	Uniform 15°	"wet" olivine[3]

[1] Shelton and Tullis [1981]

[2] Jaoul et al. [1984]

[3] Chopra and Paterson [1984]

Note: Internal angle of friction (ϕ) is lowered to implicitly include effects of ambient fluid pressure

Figure 3. Boundary conditions, initial numerical model geometry, and description of model material properties. Subduction of pro-lithosphere at 1 cm yr^{-1} occurs through basal exit region proward of prescribed point S, as indicated by velocity boundary condition at base (small arrows). Flexural compensation after incremental displacement uses a simple elastic broken beam model (parameters as for *Beaumont et al.* [1999]). Flexural response is primarily controlled by subduction load L, which represents negative buoyancy of subducted oceanic lithosphere and other slab pull forces. Shape of base owing to flexure determines direction of velocities on the base (i.e., the higher the prescribed subduction load, the steeper the exit velocities). Width of basal exit region normal to exit velocity h' is initially set to the thickness of pro-lithosphere h, so that subduction flux F_2 is equal to incoming flux F_1 but is reduced on entry of continental lithosphere and/or reduction in load L, due to flexural change in geometry which causes intersection of exit region with nondeforming retro-mantle lithosphere (see discussion in text). Model materials deform as incompressible frictional in the "brittle" or frictional regime, with Coulomb internal angle of friction parameter ϕ set to nominal value of 15°. This is lower than values measured in laboratory experiments (Byerlee's law) because it takes effect of pore fluid pressure into account implicitly. At high temperatures, deformation mechanism changes to thermally activated powerlaw creep. This change occurs at "brittle-ductile" transition and is determined dynamically as part of calculation, using flow law $\dot{\varepsilon} = A\sigma^n \exp(-Q/RT)$, where $\dot{\varepsilon}$ is strain rate, σ is stress, R is gas constant, T is absolute temperature, and parameters A, n, and Q are the preexponential constant, power law exponent, and activation energy determined from laboratory rock experiments. Upper, weak continental crust is shown on proside of model margin, but exact configuration of strong versus weak crust depends on experiment. Thermal characteristics are laterally uniform with an average linear continental geothermal gradient 20°C km^{-1}. Material operates at thermally advective limit and retains initial temperature during run, a valid approach since Péclet number is ~7 for experiments. Simple representation of surface processes, with erosion rate proportional to height of topography above baseline, denudes current topography $h_t(x,t)$ at rate $h_t(x,t)/\tau_e$ where τ_e is erosion time constant (nominal value τ_e = 1.6 Ma corresponds to moderate erosion rate). Sedimentation is neglected, except during startup phase when a small amount of trench sedimentation is used to create subduction zone geometry.

and strong continental crust. Later experiments (E5-E7) investigate more complex crustal rheologies, where upper crust has properties corresponding to "wet" quartz which may detach.

A critical assumption used in the models is that retro-mantle model lithosphere behaves rigidly and only deforms by flexural accommodation (Figure 3). This assumption is necessary because of the limited depth of the model domain. It prevents unnatural focusing of shear at the base of the model during the transition to collision. It is also consistent with inferred behavior of strong mantle lithosphere in the Alps, which (even in cases where the mantle approaches the surface as a result of inherited rift geometry) does not seem to have deformed significantly during Alpine collision. Pro-mantle lithosphere deforms with properties corresponding to "wet" olivine [*Chopra and Paterson*, 1984] but, in the cases shown

here, does not deform significantly except by passive bending and subduction.

2.3. Flux Imbalance Causing Change from Subduction to Collision

The input and subduction fluxes are $F_1 = Vph$ and $F_2 = Vph'$ respectively, where Vp is the basal velocity and h and h' are the thicknesses of the model entry and exit (Figure 3). Changes in the subduction load and in the weight of the crust both modify the subduction flux F_2 by flexing the model, thereby regulating h' and the direction of the material flow vectors at the subduction boundary. In an earlier paper [*Beaumont et al.*, 1996] dealing with dynamics of Alpine-type orogens the transition from model subduction to collision occurred as a result of a reduction in the subduction load and corresponding reduction in F_2. In fact, any process which changes model subduction geometry to reduce h' and therefore F_2 (Figure 3) will cause a corresponding change in the flux ratio (F_2/F_1) and a transition from subduction to total or partial collision. This paper investigates changes in subduction geometry and the associated change in subduction flux as a result of two distinct processes: (1) the flexural response to crustal thickness variations and (2) a discrete decrease in subduction load.

2.4. Limiting Approximations: Summary

Simplifications and approximations in the numerical models include (1) two dimensionality (models deform in plane-strain, and along-strike variations in subduction/collision dynamics are not considered), (2) limited resolution (horizontal and vertical grid spacing in the models is 2.5 and 1 km, respectively, so that kilometer-scale heterogeneities cannot be modeled, although we acknowledge that under certain circumstances these may be important controls on accretion and collision tectonics), (3) formation and exhumation of high-pressure nappes (since the maximum depth of accretion in the models is limited to the vertical depth of the model domain (nominally 60 km)), we cannot investigate the accretion and subsequent reintrusion of crustal units whose ultrahigh-pressure signatures indicate that they have been subducted to depths of 90 km or more [*Chopin*, 1984], (4) no thermal equilibration (the model advects the initial temperature distribution with no diffusion of heat), (5) no sedimentation (the effects of syncollisional sedimentation are not investigated), (6) Rigid behavior of retro-mantle lithosphere (as discussed above, retro-mantle lithosphere deforms only by flexural adjustment; as a consequence, subduction flux of pro-lithosphere is reduced for shallow subduction dips where the subducting slab intersects the strong retro-mantle), and (7) constant convergence rate (all of the experiments investigated use a constant convergence velocity of 1 cm yr^{-1}). This is a simplification compared to real orogens such as the Swiss Alps, where convergence rates estimated from tectonic reconstructions for the past 65 M-yr have varied from 1.5 to 0.3 cm/yr^{-1} [*Schmid et al.* 1997a, 1997 b]. However, Coulomb mateials, which dominate the models, are not strain rate sensitive.

2.5. Overview of Model Experiment Controls

Table 1 outlines the primary controls investigated in the model experiments. Important factors controlling dynamics include the effect of an increase in the friction between upper and lower plates during the transition from subduction of weak oceanic sediments to stronger continental crust, the effect of weak suture material on the subsequent collisional phase (E1), the effect of erosion (E1 versus E2), and the effect of a sudden reduction in slab pull forces, corresponding to inferred slab break off (E3). Several cases with more complex rheological layering are investigated in E4-E7. None of the experiments is designed to be an exact model of Alpine orogeny. Instead, the experiments investigate some of the controlling factors and the interaction between boundary forces (far-field driving stresses and subsurface loads), internal material properties

Table 1. Summary of Model Experiments[a]

Experiment	Control Investigated	Application
E1	weak suture, strong continental crust, moderate erosion	basic behavior of Alpine type orogen with weak suture and well-coupled continental crust
E2	as E1, but with no erosion	difference to E1 demonstrates the role of erosion in promoting rotation of the suture
E3	as E1, but with sudden load reduction	effect of slab break off and/or reduced slab pull force on Alpine dynamics
E4	as E1, but with weak inclusions at base of pro-upper crust	effect of heterogeneities in promoting basement nappe formation
E5	as E1, but weak retro-upper crust	detachment of upper crust and displacement of collision zone retroward; exhumation of retro-lower crust
E6	as E1, but weak pro-upper crust	weak incoming crust promotes continued subduction
E7	as E5, but includes a precursor subduction phase with entry of a small crustal terrane	accretion of a microcontinent, development of a crustal fold na collision and exhumation of accreted terrane and retro-lower crust

[a]Initial flux condition for all experiments is F_2/F_1 =100% but changes dynamically (decreases if subduction exit region intersects the position of strong retro-mantle lithosphere).

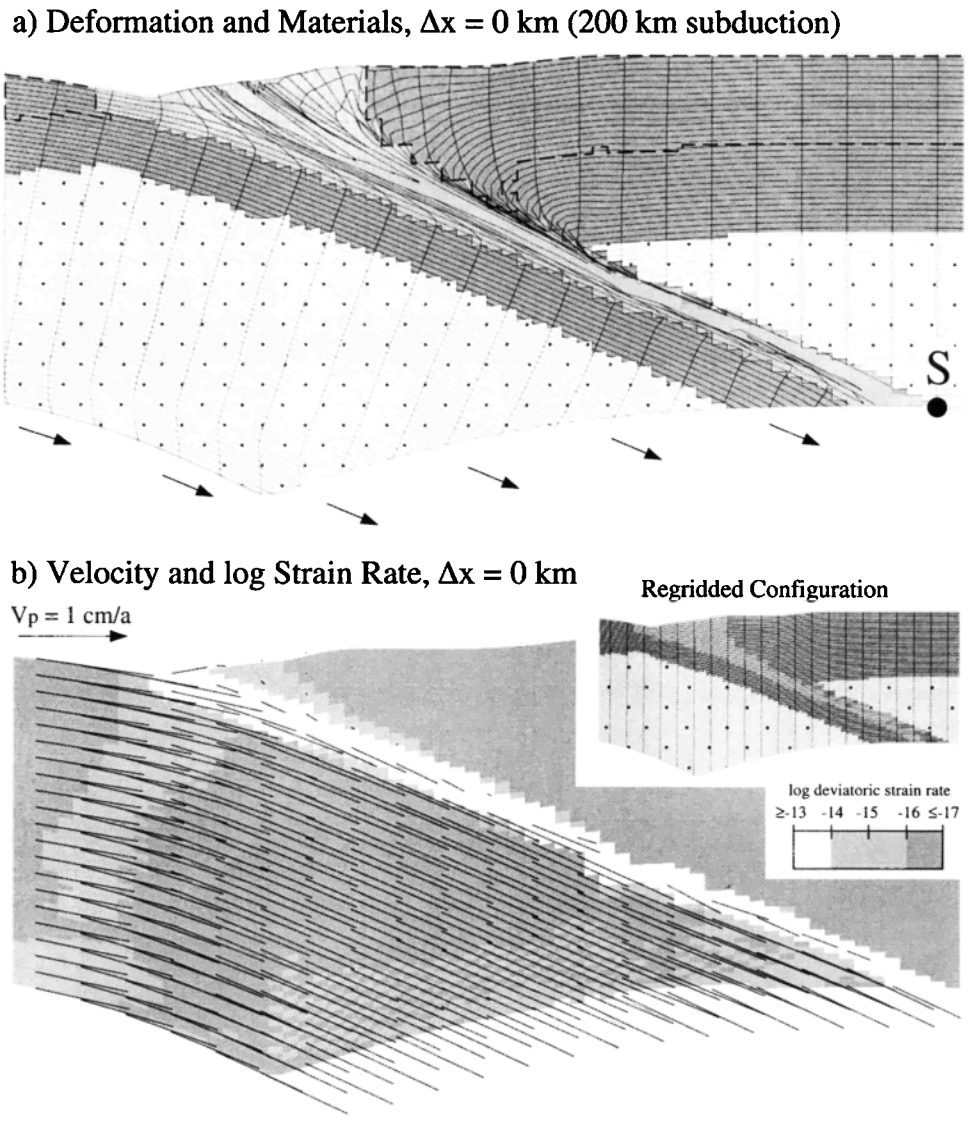

Figure 4. Starting configuration for E1 and E2. Figure in parantheses is amount of convergence during startup phase, i.e., since initial model configuration (Figure 3), and in subsequent experiments this is referred to as 0 km convergence even though there was a precursory phase. Starting geothermal gradient was linear, 20°C km^{-1}. Convergence velocity from left (proside) is 1 cm yr^{-1}, and this and subsequent model figures have no vertical exaggeration. (a) Material properties (shaded as for Figure 3) and Lagrangian (tracking) grid just before regridding to horizontal and vertical lines. Grid spacing shown is a subset of that used in the Eulerian-Lagrangian numerical computation. Dashed lines enclose regions of upper crust, which for E1, has the same properties as strong continental crust, but in later experiments may have properties corresponding to "wet" quartz. Arrows at base of Figure 4a indicate direction of exit velocity by subduction, and S indicates location of lower boundary velocity discontinuity. (b) Inset showing the same as Figure 4a but after regridding and main panel showing log second invariant of the deviatoric strain rate and velocity vectors.

(material layering), isostatic compensation, and surface processes.

3. Numerical Model Results

3.1. Experiments 1 and 2: Influence of Weak Suture Material and Erosion on Collisional Dynamics

E1 and E2 illustrate the basic dynamical modes that develop in models with strong continental crust during a transition from subduction to collision. There is no change in the subduction load L for either experiment [cf. *Beaumont et al.*, 1996]. They are identical except that E1 (Figures 4-6) has moderate denudation at a rate proportional to topographic height above baselevel (Figure 3) and E2 has no denudation (Figures 4 and 7). The initial configuration in both cases (Figure 4) is derived from a startup experiment phase, as described in section 2, and is similar to the end point of experiment R1 by *Ellis et al.* [1999].

E1 undergoes a transition from model subduction to

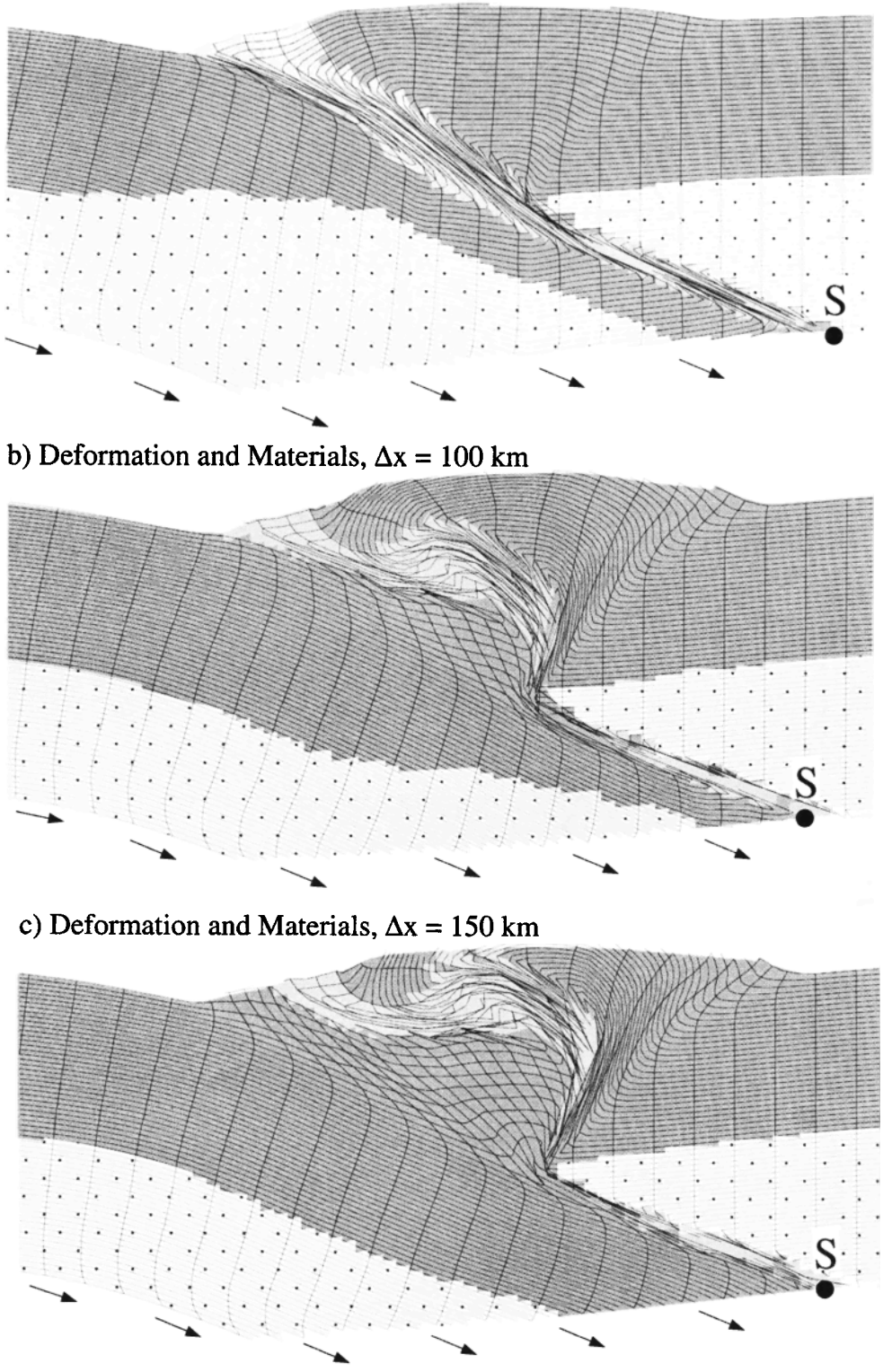

Figure 5. E1 with strong crust, weak suture, and moderate erosion, showing evolution in material property distribution and tracking grid for nominal behavior of a model undergoing transition from subduction to collision. Advection of weak material into retroshear zone and elevation-dependant erosion drives rotation of the plug, causing the suture material to eventually lie flat at the surface. Shadings and material properties are as indicated on Figure 3, and boundary conditions and location of velocity discontinuity at base (S) are shown on each panel. All other properties are as for Figure 4. Tracking grid was regridded to horizontal and vertical lines at 0 km convergence as shown in Figure 4. Thick line on grid indicates datum line that was initially horizontal at 10 km depth.

d) Deformation and Materials, Δx = 200 km

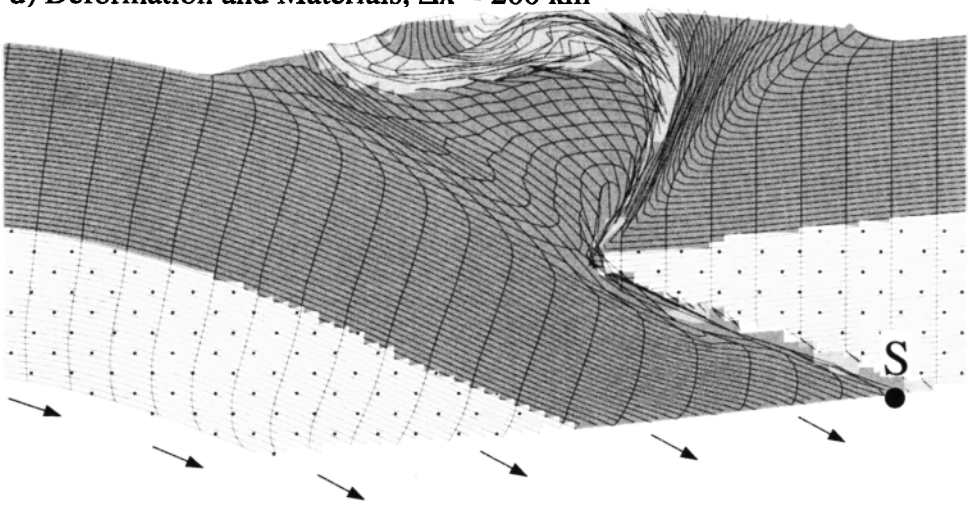

e) Deformation and Materials, Δx = 250 km

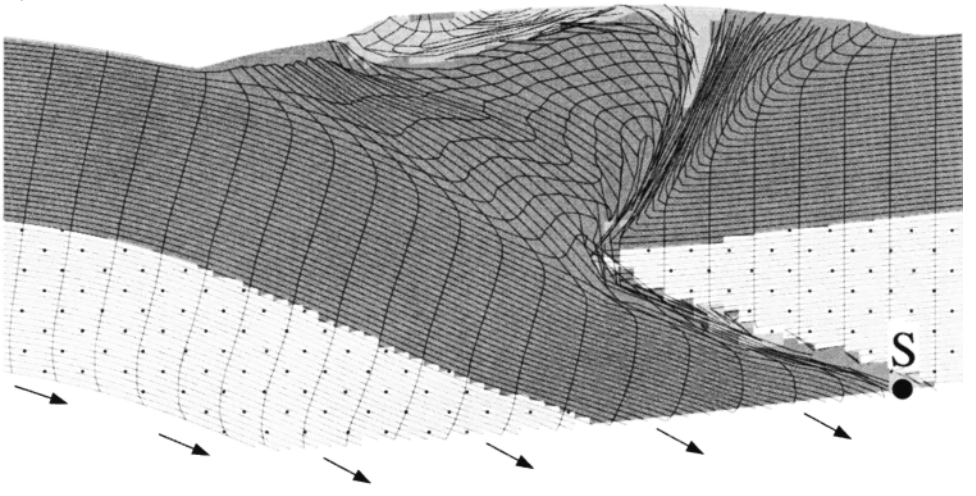

f) Deformation and Materials, Δx = 300 km

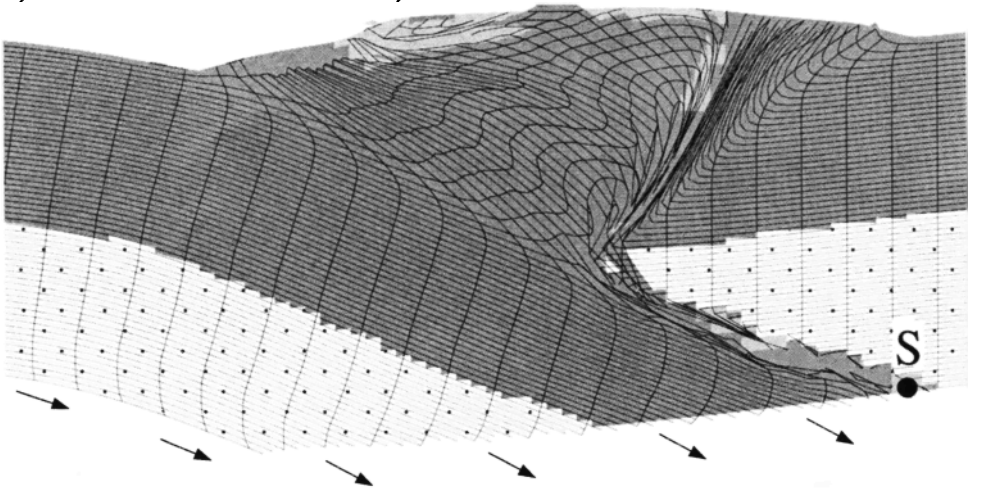

collision as a result of the entrance of strong, well-coupled continental crust into the model subduction zone (Figures 5a and 5b). The topography at the start of the experiment has a small wedge of suture material overlying the subduction interface, which lies at a critical and stable geometry for $\phi = \phi_b = 9°$. During the transition period (Figures 5a and 5b), the frictionally weaker suture material is sheared at the interface between upper and lower plates. The transitional dynamics can be understood in terms of critical wedge theory [e.g., *Davis et al.*, 1983, figure 8]. Entrance of strong continental crust into the model subduction zone at 50-150 km convergence changes the basal angle of friction for the accreting wedge from $\phi_b = 9°$ (suture material) to $\phi_b = 15°$ (strong continental crust). The critical taper increases because the proward end of the suture material is dragged downward, and simultaneously, crustal material is underplated beneath the hanging wall. The net effect is to rotate the suture counterclockwise (Figure 5c) and cause the locus of uplift to shift retroward. The trench region actually deepens because of enhanced downward shearing of suture material. Flexural adjustment to the shift in locus of topographic load retroward causes a shallowing in the subduction angle so that the subduction exit region intersects the rigid retro-mantle lithosphere. This dynamic behavior of the model reduces the subduction flux to ~80% of incoming flux.

The simplified flexural model can be interpreted to represent the combined effects of the gradual decrease in slab load or increased buoyancy of continental crust. Sudden reductions in flexure (representing slab break off [cf. *Davies and von Blanckenburg*, 1995]) are investigated in E3.

The frictionally weak suture material not only affects dynamics during the transition from subduction to collision in E1 but also influences the subsequent evolution of the model. Figure 6 shows that deformation and shortening within the incoming (pro) model continental lithosphere does not occur in a distributed fashion but remains focused within the suture zone until ~100 km of convergence. After this point, the suture material has been advected upward (by underplating and denudation at the surface), so that it can no longer be used by the pro-step-up shear zone. There is a jump in the position of the pro-shear zone into the stronger continental crust, and distributed retroshear leads to a crustal-scale backfold within the uplifted model continent, which can be seen most clearly during the last phase of the experiment (Figure 5f). The weak suture material is passively rotated into this backfold which has a limb that lies almost horizontally at the surface (Figure 5f).

In E1, continuous elevation-dependant erosion not only leads to rotation and exposure of suture material at the surface after 250 km of convergence (Figure 5e) but prevents a large topographic load from developing (maximum thickness of retro-crust in the model is ~70 km). In contrast, E2 has no denudation and does not experience the later phase of rotation (compare Figures 5e and 7b). It develops a large topographic load, where maximum retro-crust thickness exceeds 85 km. The thicker crust loads down the model margin so that the dip of the upper-lower plate interface is ~30°, and the flexural response is enough to change the subduction geometry so that subduction flux balances incoming flux again. E1 and E2 therefore demonstrate the feedback between dynamics, erosion, and flexure during the transition from subduction to collision. In the case with erosion, a dynamic steadystate is achieved, with a flux balance between incoming material and mass lost by erosion and partial subduction, and a constant topographic profile. With no erosion, a different steady state balance results, where incoming material flux equals mass lost by subduction.

3.2. Experiment 3: A Sudden Decrease in Subduction Load

E3 is initially identical to E1. Between 50 and 58 km of convergence, E3 experiences a sudden reduction in subduction load by 50% (Figure 8). The subduction load represents the vertical component of the slab pull force. Its sudden reduction corresponds to subsurface unloading effects (e.g., slab break off) during the transition from subduction to collision at a convergent margin. After unloading, the dynamics of the system (Figure 8) are completely changed compared to E1 (Figure 5). The flux imbalance between incoming (pro) material and subduction exit grows to 50%, causing a phase of increased uplift in the overlying retro-crust. The entire plug region is uplifted and exhumed, with little rotation of the crust and suture (Figure 8e). The suture material is passively advected toward the surface, retaining its original dip even near to the retroshear zone, and is gradually lost by erosion. Although E3 attains a dynamic steady state like E1, the two patterns of exhumation differ significantly.

3.3. Experiment 4: Effect of Weak Inclusions Within the Pro-Lithosphere

Considering the heterogeneous nature of continental lithosphere and the distribution of lithologic units within orogenic belts, it is to be expected that heterogeneities may be important to the overall development of an orogen. A simple example is provided by E4, which investigates the effect of several regularly spaced rectangular weak inclusions embedded within the incoming pro-lithosphere (Figure 9). They have ductile properties corresponding to laboratory measurements for "wet" quartz [*Jaoul et al.*, 1984], allowing them to deform in the ductile field at depths between 12 and 15 km in the model, which has a linear continental geothermal gradient of 20°C/km. In contrast, the surrounding, strong continental model crust (with ductile properties of feldspar x 10) deforms as a frictional material.

The early dynamics (not shown) are similar to E1 (Figure 5a). After 100 km of convergence, proward shear is progressively focused within and around each approaching inclusion, causing limited decoupling at the mid-crust. Sequential jumps in the focus of shearing from one weak zone to the next causes the development of major crustal-scale folds within the pro-crust, as can be seen from the initially horizontal and vertical lines in the tracking grid in Figures 9a, 9b, and 9d. The weak material forms the core of the emerging antiforms and resists subduction. Nevertheless, the weak zones are eventually subducted because they are sufficiently deep, but they leave behind a record of their passage in the complexly deformed uplifted plug (compare with E1, Figure 5). In other cases, less deeply buried weak zones may be accreted within the pro-wedge. Between 100 and 250 km of

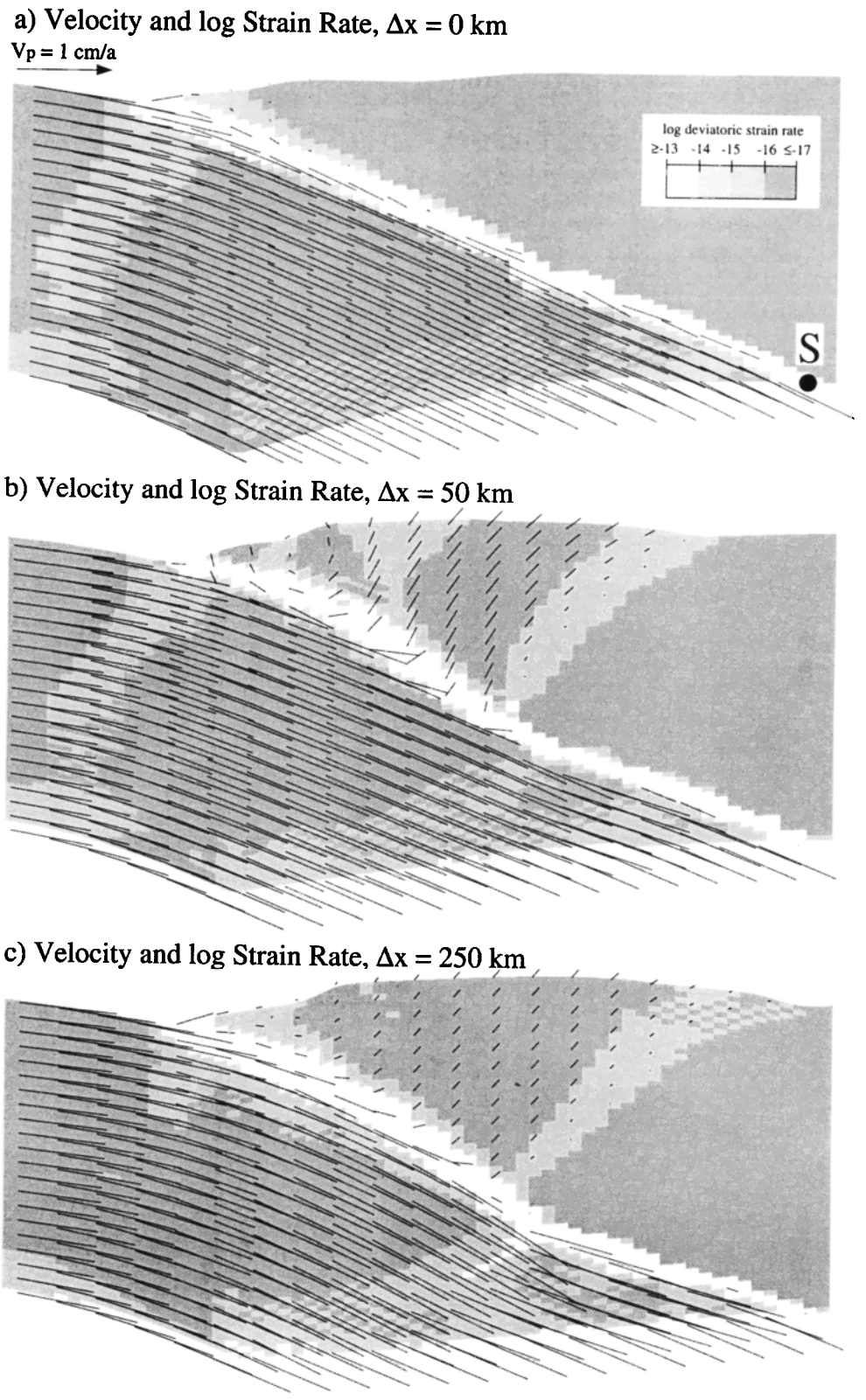

Figure 6. Velocity vectors and log second invariant of the deviatoric strain rate for E1 at three selected convergence states. Note deflection of material trajectories from incoming lithosphere toward the upper plate, causing plug uplift.

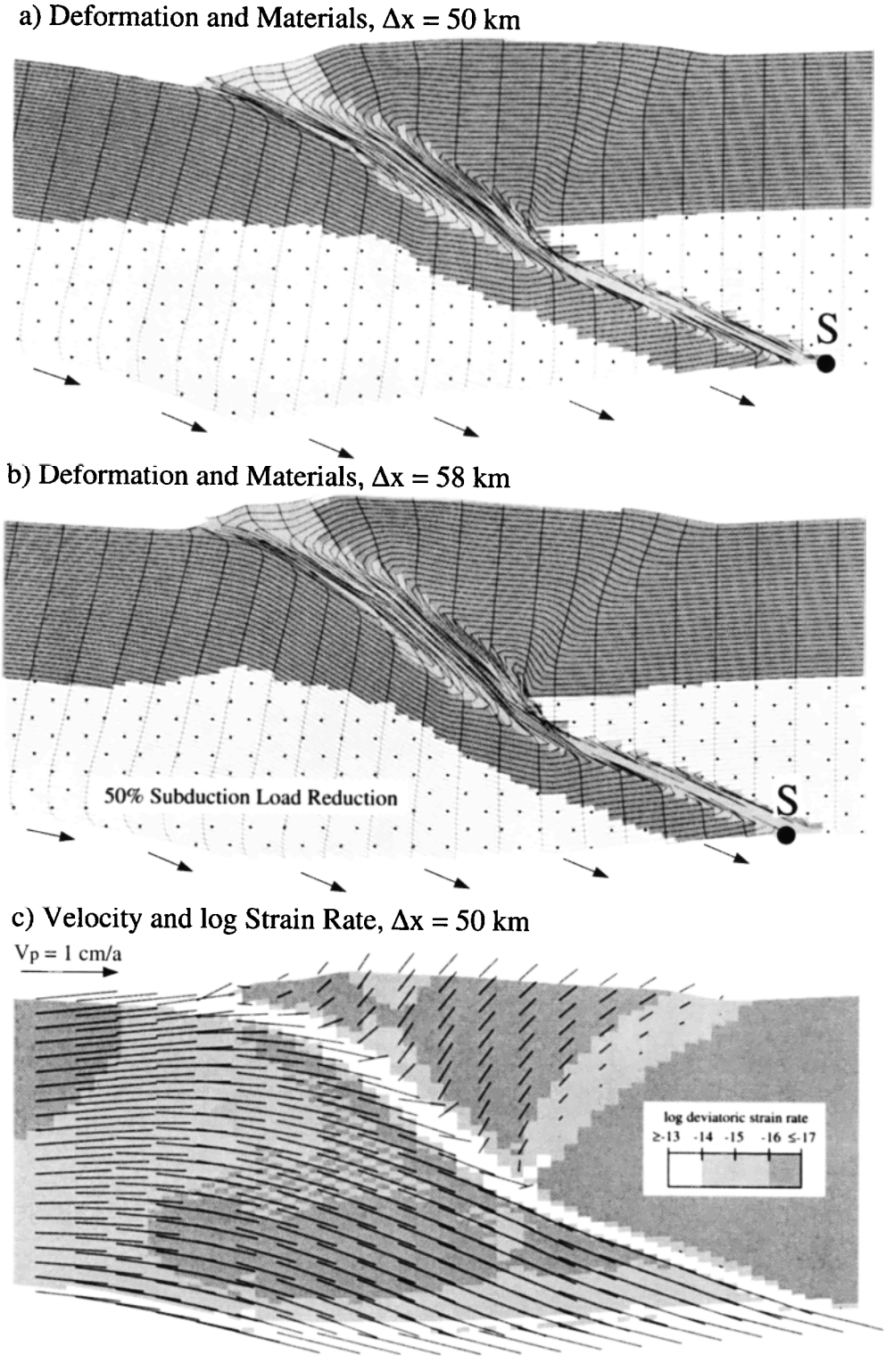

Figure 7. E2 with strong crust, weak suture, and no erosion. (a and b) material properties and tracking grid and (c) velocity vectors and log second invariant of the deviatoric strain rate. All other symbols and shadings are as for Figure 4. Thick line on grid indicates datum line that was initially horizontal at 10 km depth.

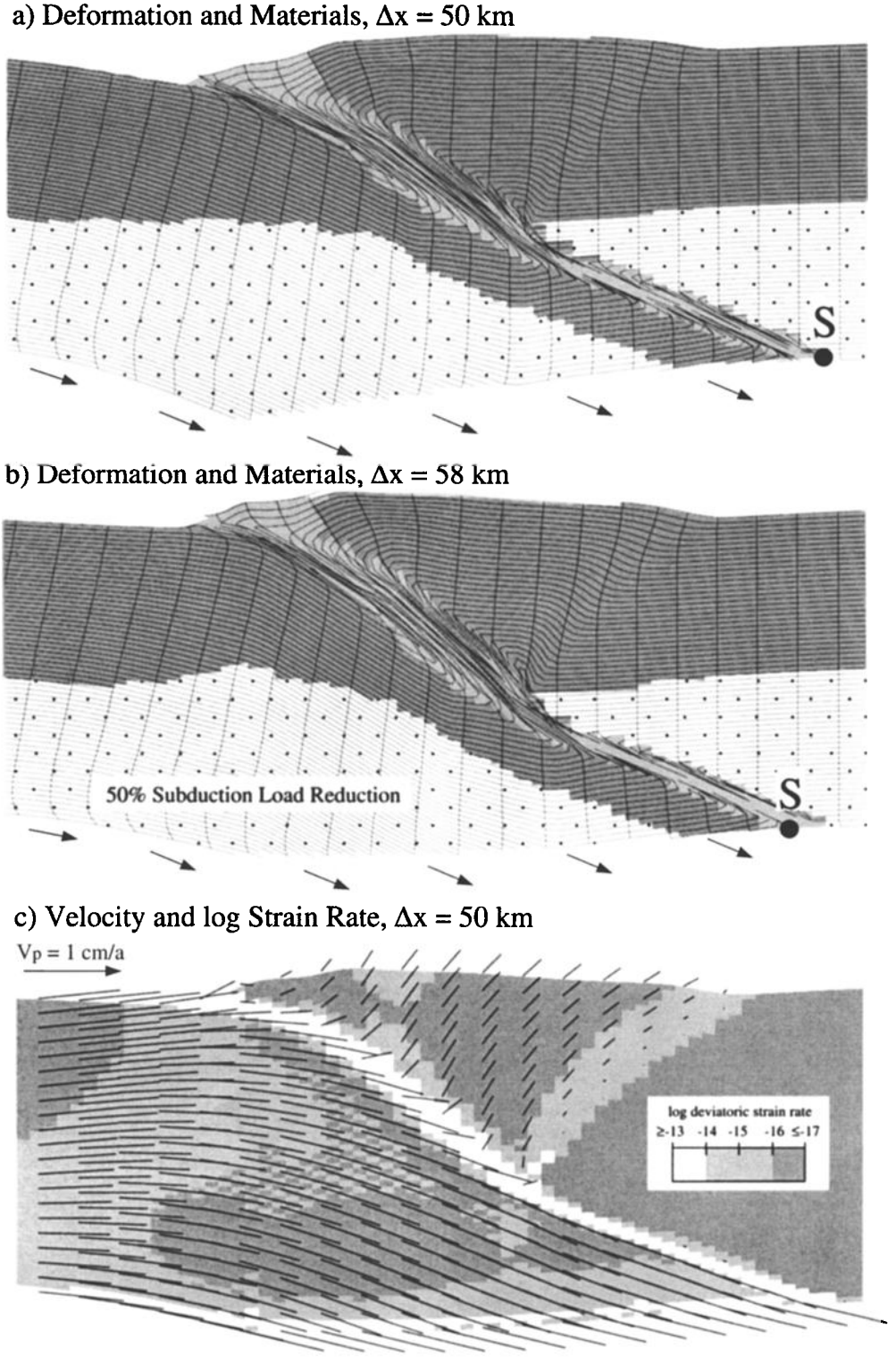

Figure 8. E3 with strong crust, weak suture, and moderate erosion with rapidly reduced subduction load, showing material properties and tracking grid (Figures 8a, 8b, 8d, and 8f) and velocities/log second invariant of deviatoric strain rate (Figures 8c and 8e). Subduction load was reduced to 50% of its initial value between 50 and 58 km of convergence. All other parameter values are as for E1, and symbols and shadings are as for Figure 4. Thick line on grid indicates datum line that was initially horizontal at 10 km depth.

d) Deformation and Materials, Δx = 150 km

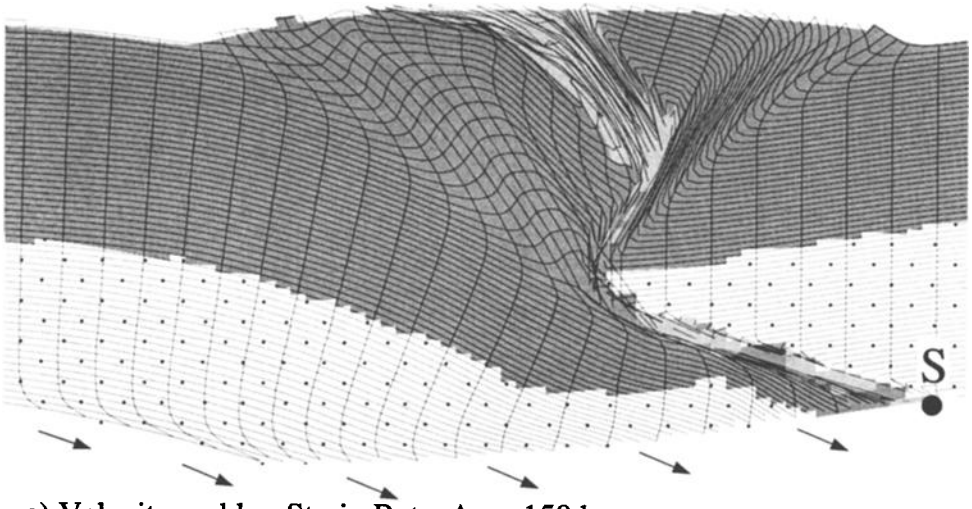

e) Velocity and log Strain Rate, Δx = 150 km

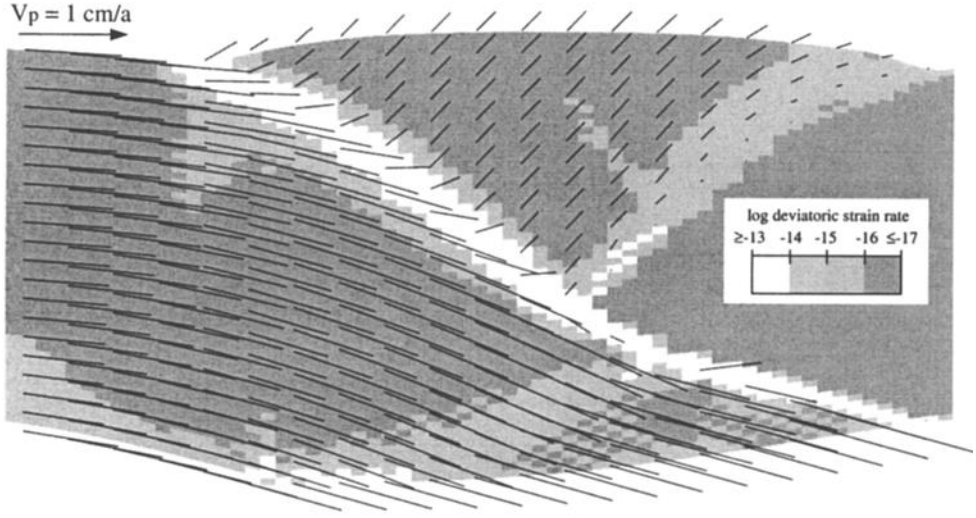

f) Deformation and Materials, Δx = 250 km

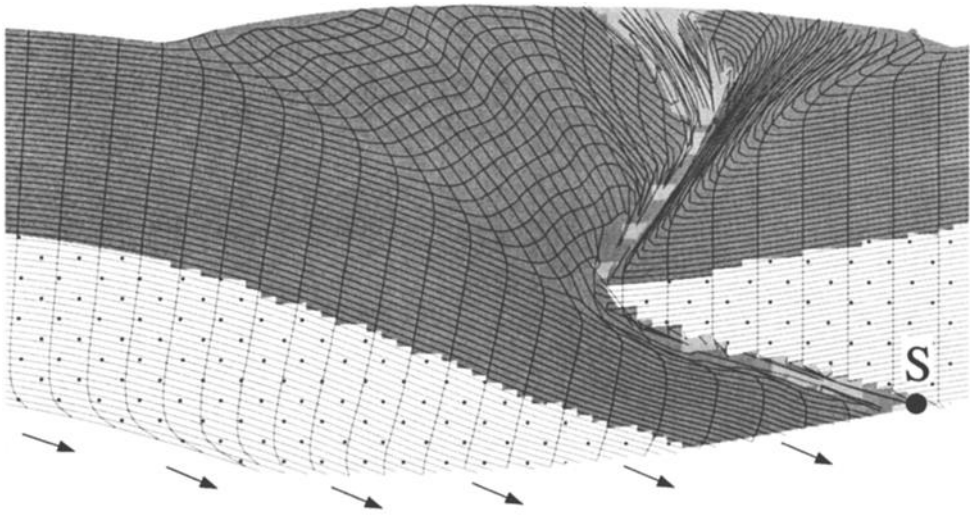

Figure 8. (continued.)

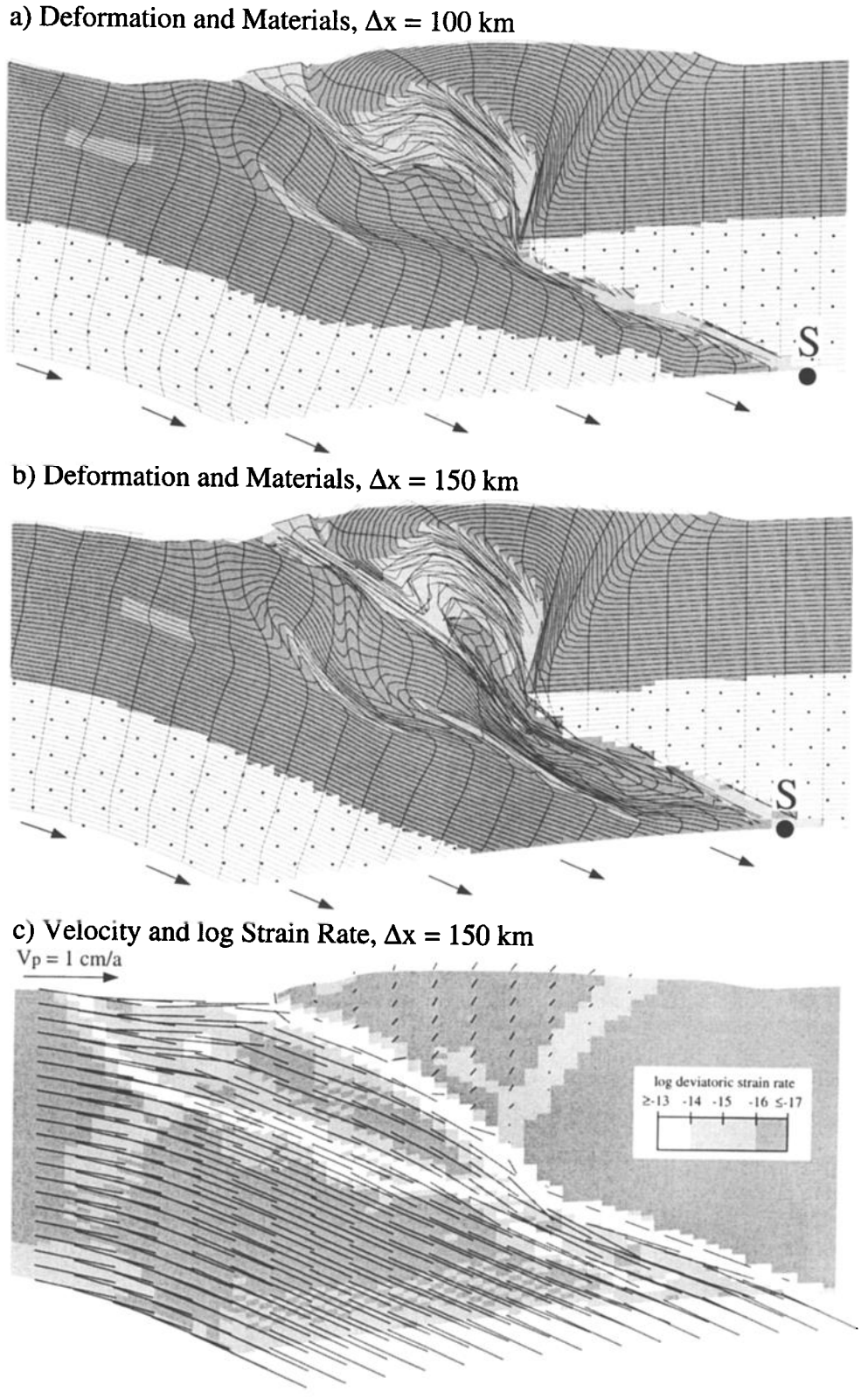

Figure 9. E4 with weak inclusions in strong pro-crust, weak suture, and moderate erosion, showing material properties and tracking grid (Figures 9a, 9b, and 9d) and velocities/log second invariant of deviatoric strain rate (Figures 9c, 9e). Rectangular inclusions have ductile properties of "wet" quartz *[Jaoul et al.*, 1984] and are initially at 12-15 km depth, 10 km wide, and separated by 30 km of normal (strong) continental crust. Note higher strain rates within weak zones.

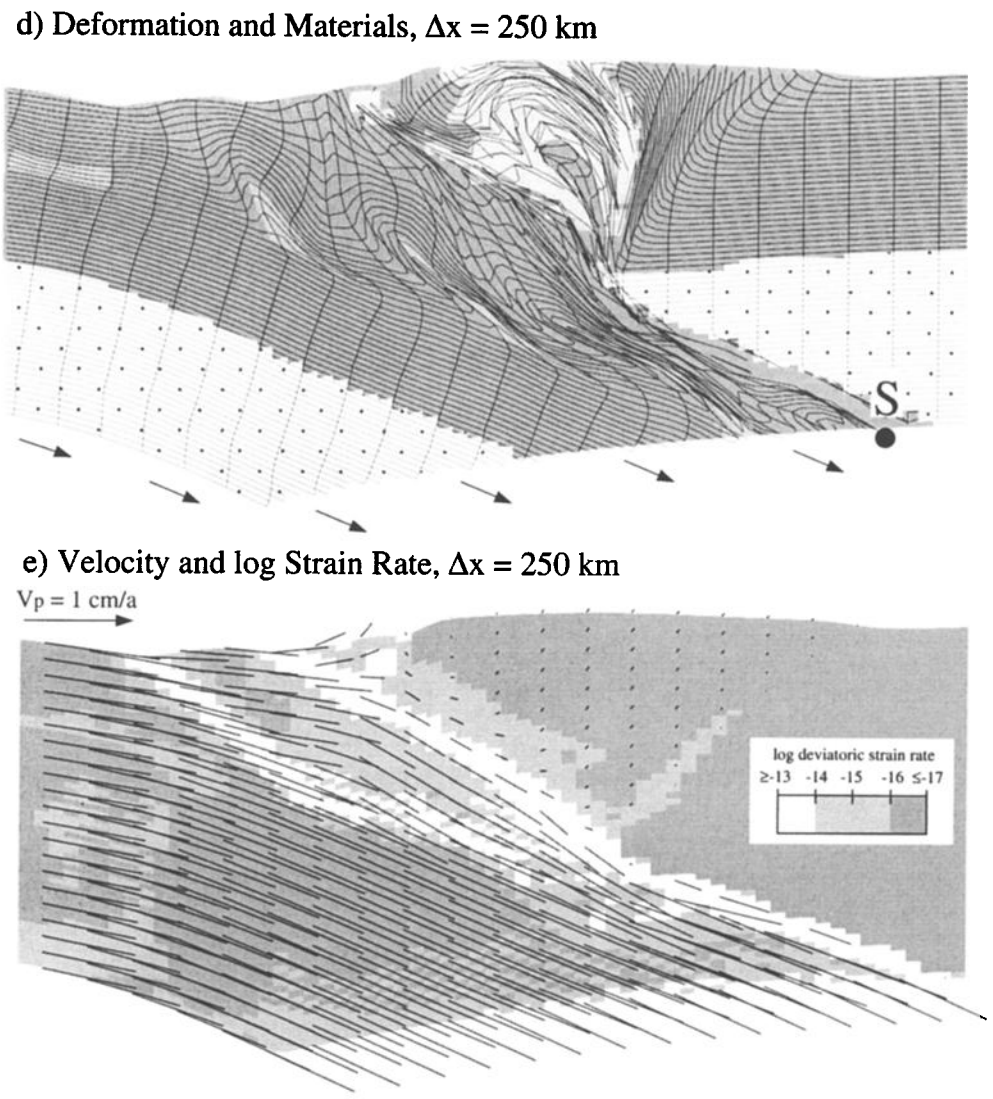

Figure 9. (continued.)

convergence, shear interaction between the weak suture material and the leading weak zone allows suture material to be wrapped around a small segment of model continental upper crust.

The deformation in the uplifted plug takes the form of a series of crustal-scale fold nappes. Fold nappes are the closest that a continuum finite element model can come to modeling thrust sheets bounded by discrete (thrust) faults.

The final configuration after 250 km convergence differs from the simpler experiment (E1) because the suture material has not been rotated, and the uplifted pro-crustal layer has a series of stacked, crustal-scale folds within it. Although E4 provides only one simple, specific example of the effect of heterogeneous strength within incoming continental crust, it demonstrates that the presence of weak zones may alter crustal dynamics significantly.

3.4. Experiment 5: Effect of Weak Upper Crust Within the Retro-Lithosphere

In E5 we investigate the effect that a midcrustal local strength minimum in the retro-crust would have on a model that is otherwise identical to E1. Shallow retro-crustal strengths are frictional (as in E1), whereas "wet" quartz ductile behavior dominates at midcrustal level. The early stages (Figure 10a) are not significantly different to earlier experiments. Once collision has been initiated by entry of strong pro-crust into the model margin, a detachment between retro-upper and lower crust is activated by the weak ductile horizon at the base of the retro-upper crust, leading to the formation of a crustal-scale synclinal structure in the retro-crust (Figures 10c, 10d, and 10f). Its horizontal limb is transported retroward, and its steep limb is uplifted with an opposite shear sense along the midcrustal detachment. The kinematics resemble those of folds in multilayers undergoing bedding-parallel slip [e.g., *Ramsay* , 1967].

The uplifted and exhumed model pro-crust and suture are transported retroward over the lower parts of the retro-lithosphere (Figures 10d, and 10f). The suture material is rotated and exhumed as in E1. In addition a small piece of retro-lower crust is uplifted, deformed, and rotated in the footwall of the retro-step-up shear. Most of the retro-lower crust remains undeformed and sits passively beneath the

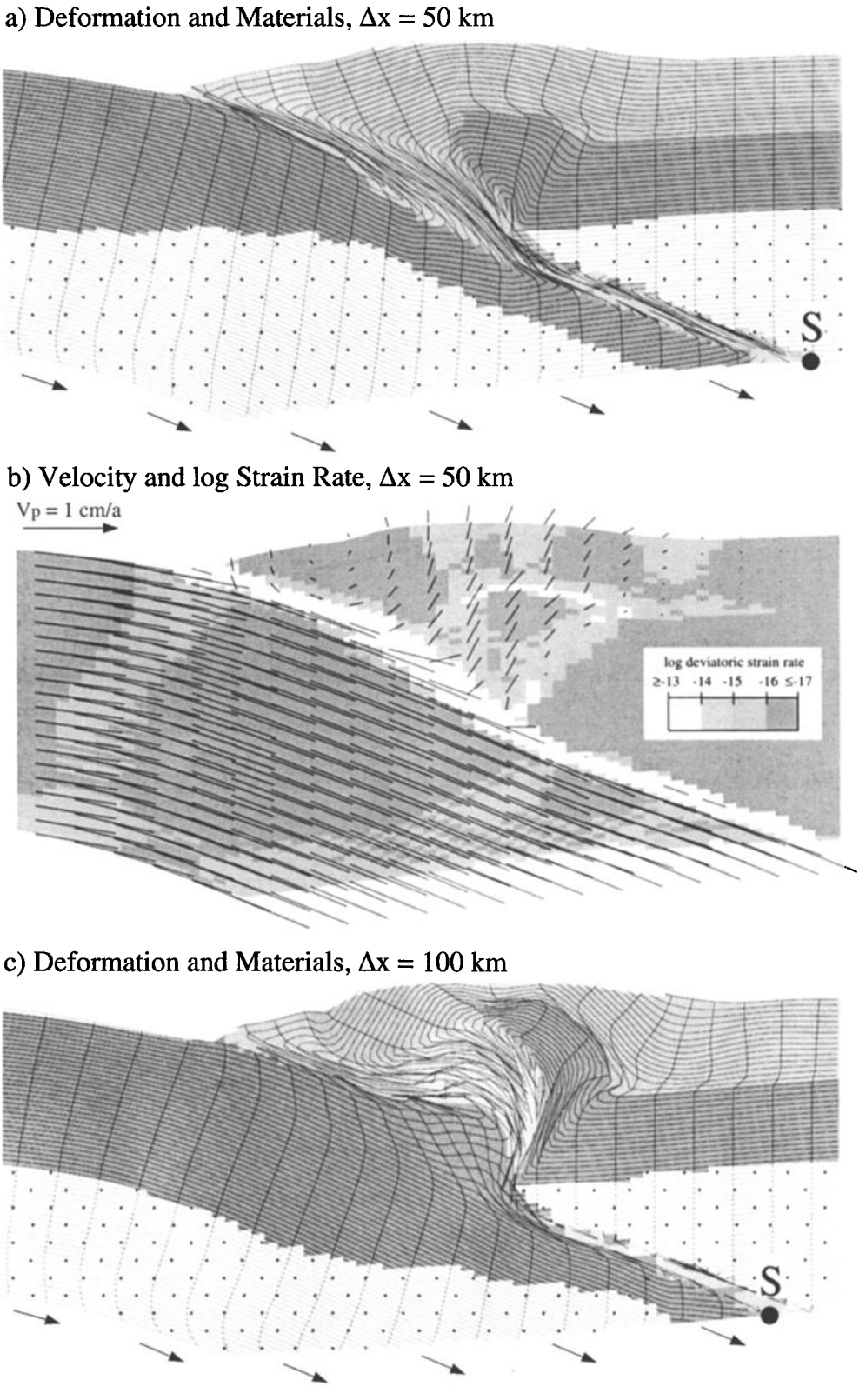

Figure 10. E5 with weak retro-upper crust, weak suture, and moderate erosion, showing material properties and tracking grid (Figures 10c, 10d, and 10f) and velocities/log second invariant of deviatoric strain rate (Figures 10b, and 10e). Properties are the same as E1 except that retro-upper crust (thickness 15 km) has ductile properties corresponding to "wet" quartz.

d) Deformation and Materials, Δx = 200 km

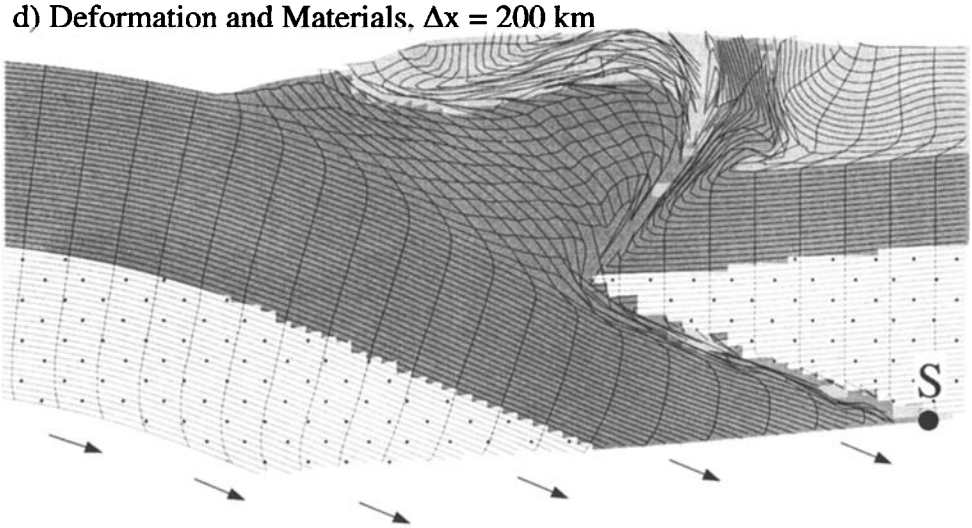

e) Velocity and log Strain Rate, Δx = 200 km

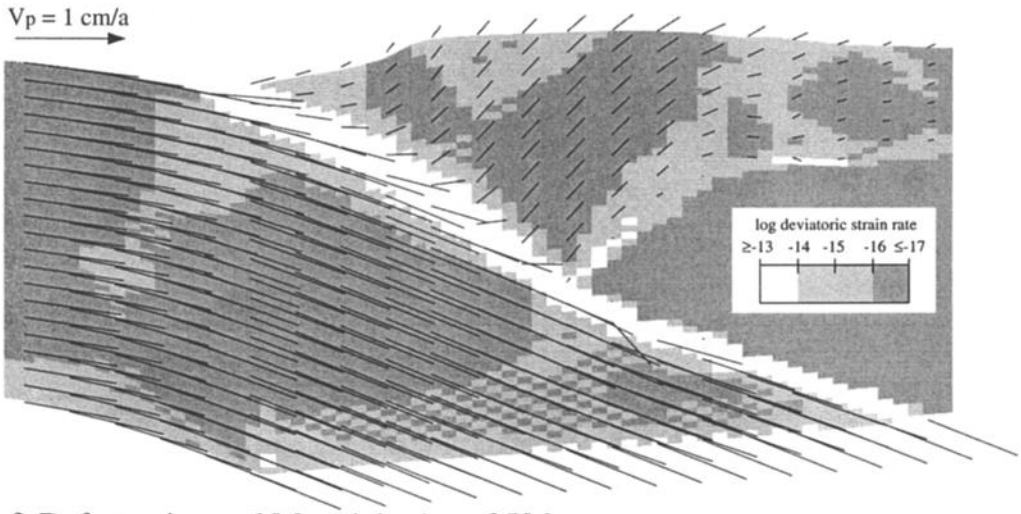

f) Deformation and Materials, Δx = 250 km

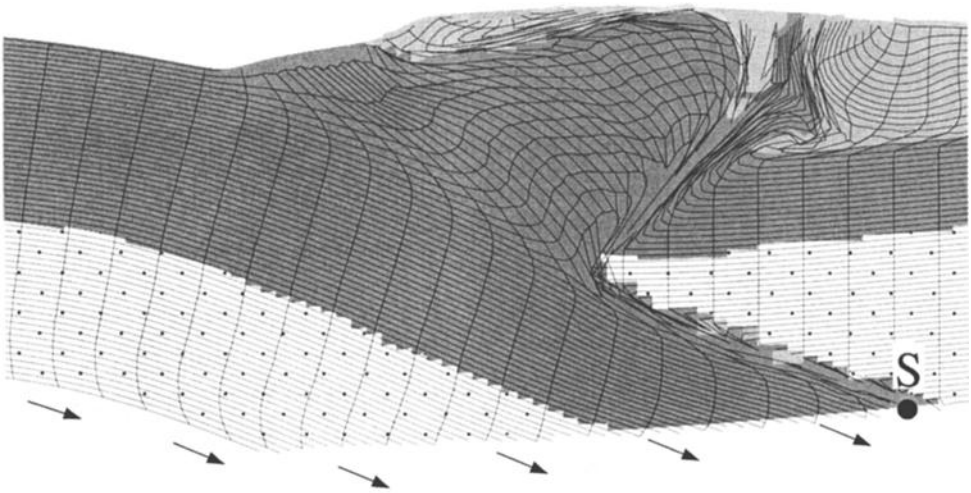

Figure 10. (continued.)

collision zone, giving it the geometry of an apparent lower crustal indenter. The material properties of retro-lower crust are the same as in previous model experiments, and the "apparent indentation" is a result of deformation that is focused within the weak ductile region at the base of the retro-upper crust. A tilted section of the model lower crust is exposed at the surface sandwiched between the retro-upper crust and the suture material (Figures 10d, and 10f).

3.5. Experiment 6: Effect of Weak Upper Crust Within the Pro-Lithosphere

E6 investigates a contrasting end-member to E5, where an equivalent ductile strength minimum occurs in the pro-crust instead of the retro-crust (Figure 11). The change in dynamics after collision begins is quite marked compared to E1. Detachment at the base of the pro-upper crust starts as the pro-continent enters the model subduction margin, causing crustal thickening and deformation to propagate proward. The proward thickening and loading changes the flexural response of the margin. This in turn opens the subduction exit region so that subduction flux F_2 eventually balances incoming flux F_1. As a result, uplift is suppressed, suture material is not exhumed to the surface, and an orogen corresponding to this model end-member would exhibit deformation and thickening over a wide area proward of the suture zone.

3.6. Experiment 7: Collision With Complex Suture Zone Including Accretion of a Microcontinent

The final model experiment combines properties from the previous experiments with some of those from *Ellis et al.* [1999] in order to investigate the accretion of a microcontinent followed by collision. It is the same as E5 (strong pro-crust, weak retro-crust; see Figure 3) except that there is a precursor terrane accretion phase. Closure of a 250 km wide precursor model ocean with a weak frictional sediment layer (phase 1, not shown) is followed by phase 2, the entry of a small continental terrane (Figures 12a, and 12b). The terrane has a weak upper crust which detaches at the midcrustal strength minimum, is accreted at the subduction zone, and is deformed into an overturned crustal-scale fold (as explained more fully in similar experiments by *Ellis et al.* [1999]). Tectonic underplating of the fold beneath the model subduction margin during phase 3 (150 km convergence, Figure 12c) is accompanied by uplift, even though the subduction flux remains at 100% of incoming flux. This is possible because of a transition from a mode of pure subduction of all incoming material to a "transient blockage" mode with reduced loss of material from the subduction conduit below (P-U-C mode in the terminology of *Beaumont et al.* [1999]). The shift in dynamics allows the model subduction zone to accrete the upper units of the crustal terrane [cf. *Ellis et al.*, 1999], while its leading and trailing edges are subducted.

During phase 3, further oceanic subduction occurs, and a new accretionary wedge is grown (Figure 12c). In phase 4 (after 200 km of convergence), continental lithosphere enters the subduction zone and collision begins. The transition to collision with strong continental crust reinitiates retrothrusting of the nappe and surrounding suture material, which are gradually rotated and exhumed (Figures 12d-12f). Crustal thickening attains a maximum value of 70 km (Figure 12f). The accreted microcontinent is exhumed to the surface, partly by denudation and partly by extension in the upper part of the plug (see later). Figure 12f shows a small piece of retro-upper crust which was initially located in the upper plate but is now at the top of the uplifted plug and has been rotated counterclockwise. Owing to denudation this piece is now isolated from the rest of the retro-upper crust, and is underlain by suture material, giving the appearance of a klippe. The final geometry of the deeper parts of the model orogen after 300 km convergence is very similar to E5 at 200 km convergence (Figure 12f, compare Figure 10d).

Overall, E7 demonstrates a mechanism by which a complex juxtaposition of units can be achieved by subduction, accretion, tectonic underplating, and retrothrusting. Of particular interest is the model surface "geology" at 250 km of convergence (Figure 12e), which exposes pro-continental crust, accretionary wedge sediments (derived from both oceans), retro-upper crust, pieces of the accreted microcontinent, and lower and upper retro-crust. As noted below, this tectonic assemblage can be regarded as a prototype of that observed in some Alpine crustal cross sections.

4. Case History of the Evolving Swiss Alps

The Alps evolved from two orogenies: the first in the Cretaceous, the second in the Tertiary [*Schmid et al.*, 1996, 1997a, 1997b; *Stampfli and Marchant*, 1997; *Stampfli et al.*, 1998]. The two plates involved, the European and Adriatic plates, had a curved plate boundary defining an east dipping subduction beneath the Western Alps in the Cretaceous, changing to a south dipping subduction beneath the Swiss Alps in the Tertiary. The Cretaceous orogeny was characterized by top to the west and WNW imbrications, orogen-parallel strike-slip movements including motion along a paleo-Insubric Line [cf. *Pfiffner*, 1992], thrusting in the Southern Alps [*Doglioni and Bosellini*, 1987], high-pressure metamorphism, subduction of oceanic fragments in the Eastern Alps (Austria), and subduction of oceanic fragments and an extensional margin in the Western Alps (France/Italy, Sesia zone). This eoalpine orogeny is not discussed further in this paper. A Late Cretaceous extensional phase marks the transition between the two orogenies, with normal faulting at higher levels and folds with horizontal axial surfaces below [*Froitzheim et al.*, 1994].

The Tertiary orogeny had a north to NNW directed convergence. On the basis of the type of material entering the south dipping subduction zone and the evolving subduction geometry, three phases can be distinguished: (1) subduction of oceanic crust (Piemont ocean), (2) underplating of continental fragments (Briançonnais microcontinent), and (3) collision phase (European continental margin, 195 km of convergence). Only the last, Neogene collisional phase is compared to the modeling presented in this paper. Modeling of the subduction phase is discussed in *Beaumont et al.* [1999], and tectonic underplating of continental fragments is discussed by *Ellis et al.* [1999].

In order to compare the model results with the evolution of the Alps a number of palinspastic, retrodeformed cross

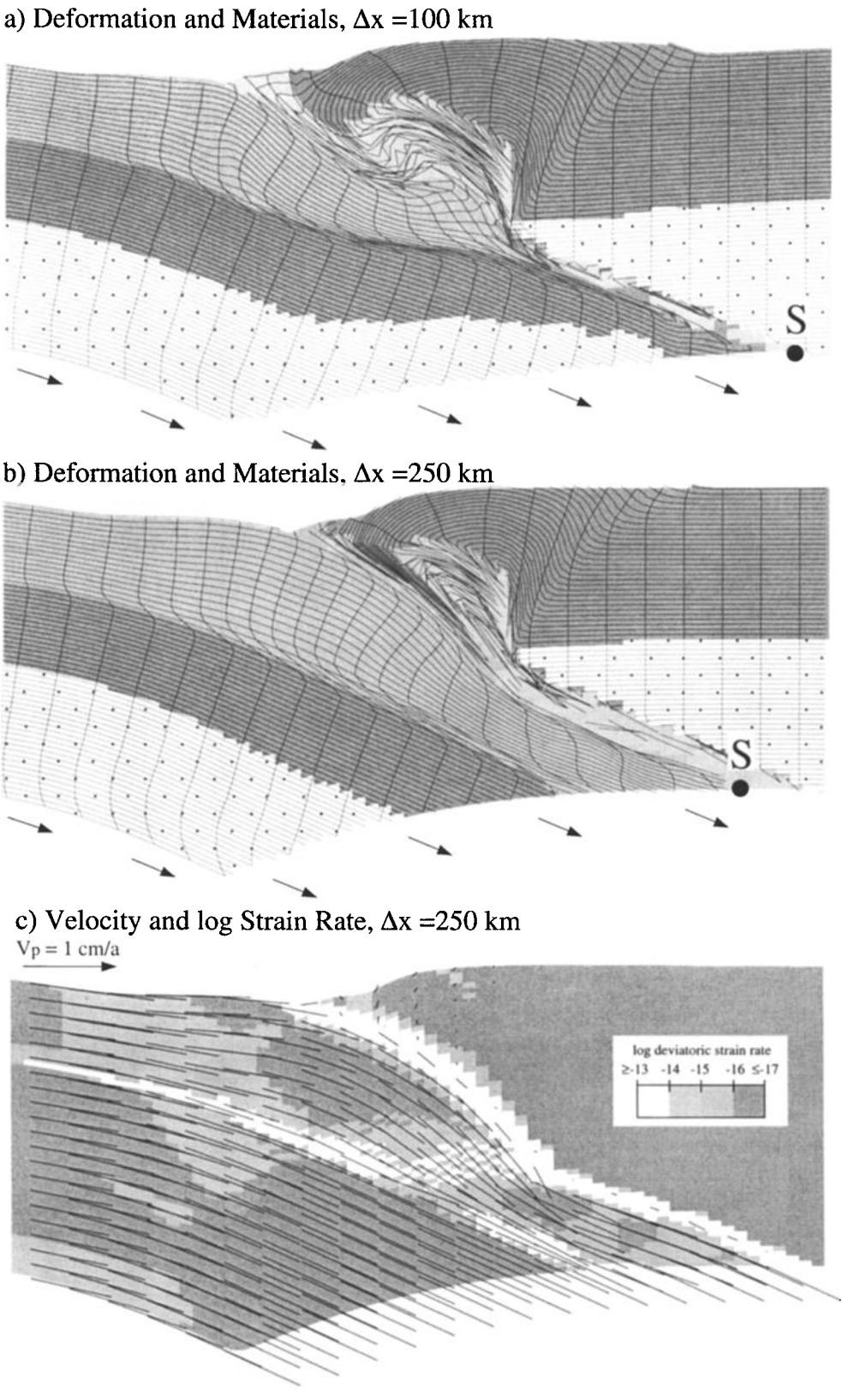

Figure 11. E6 with weak pro-upper crust, weak suture, and moderate erosion, showing (a and b) material properties and tracking grid and (c) velocities/log second invariant of deviatoric strain rate. Properties are the same as E1 except that pro-upper crust (thickness 15 km) has ductile properties corresponding to "wet" quartz.

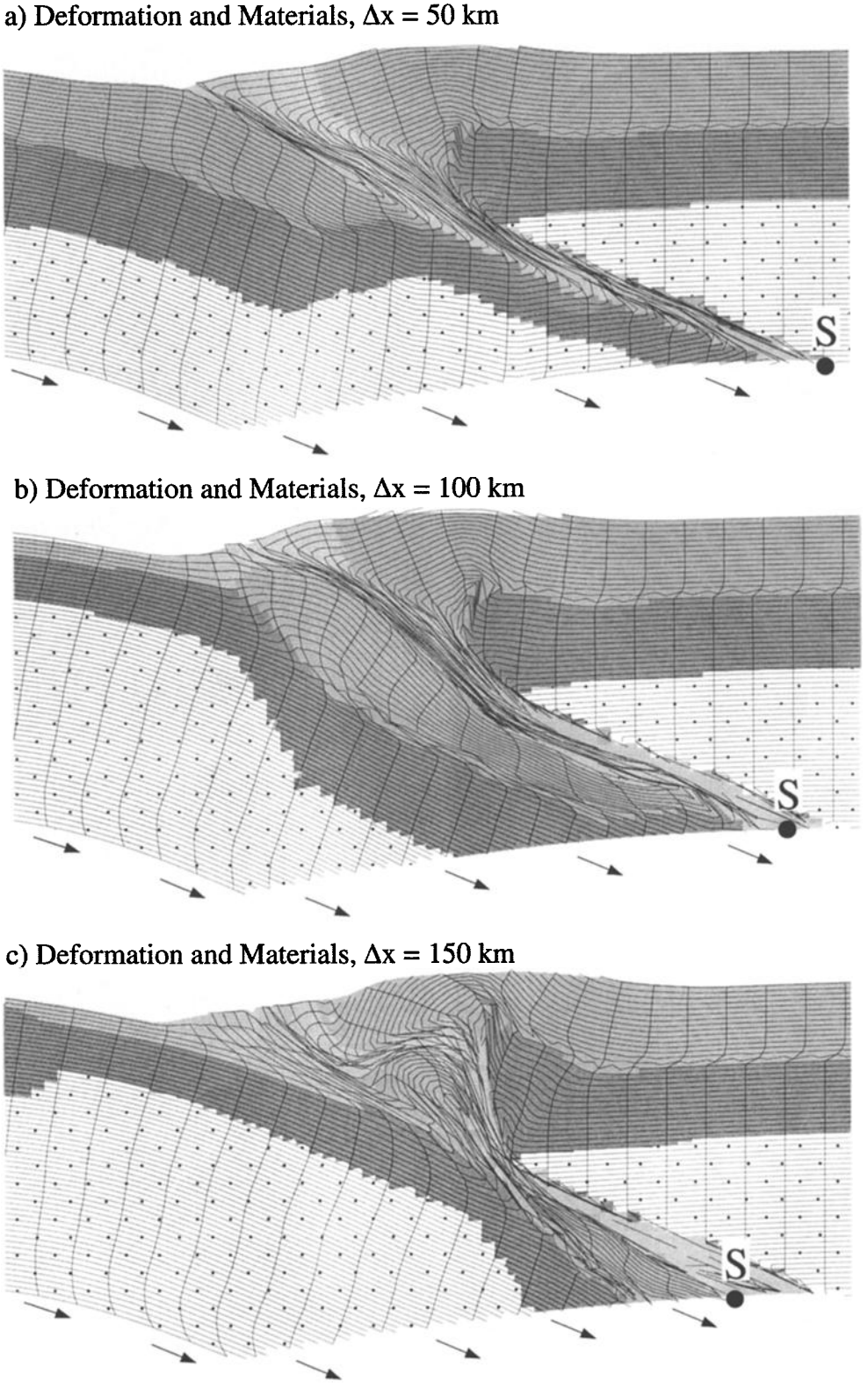

Figure 12. Evolution in material properties and tracking grid for E7. Precursor phase subducts and underplates upper units of a small, detachable continental terrane (50-150 km convergence). Terrane has 15 km thick upper crust with ductile properties of "wet" quartz and 15 km thick lower (strong) continental crust. Terrane width is 50 km with 20 km wide transition regions where crust thins from 30 to 15 km. Underplating is followed by transition to collision as strong uniform continental crust enters the model margin (> 200 km convergence). Erosion rate and all other parameters are the same as for E1.

d) Deformation and Materials, Δx = 200 km

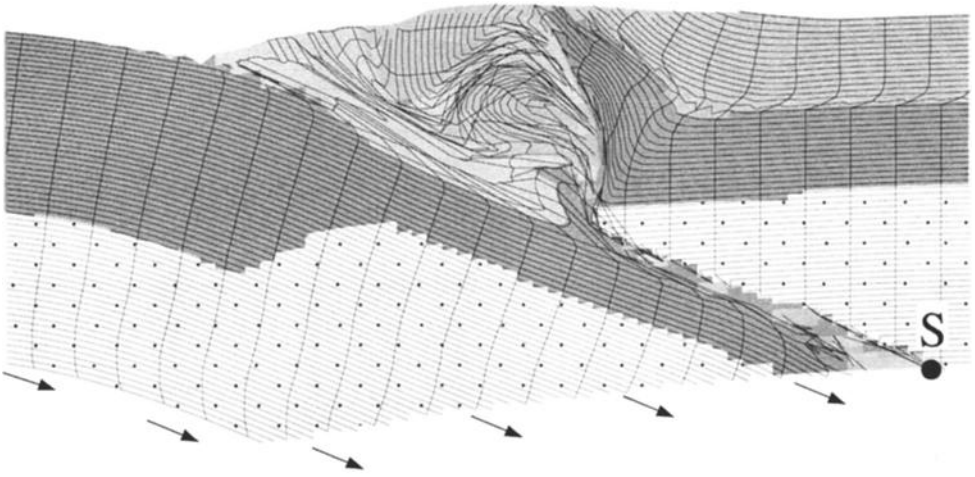

e) Deformation and Materials, Δx = 250 km

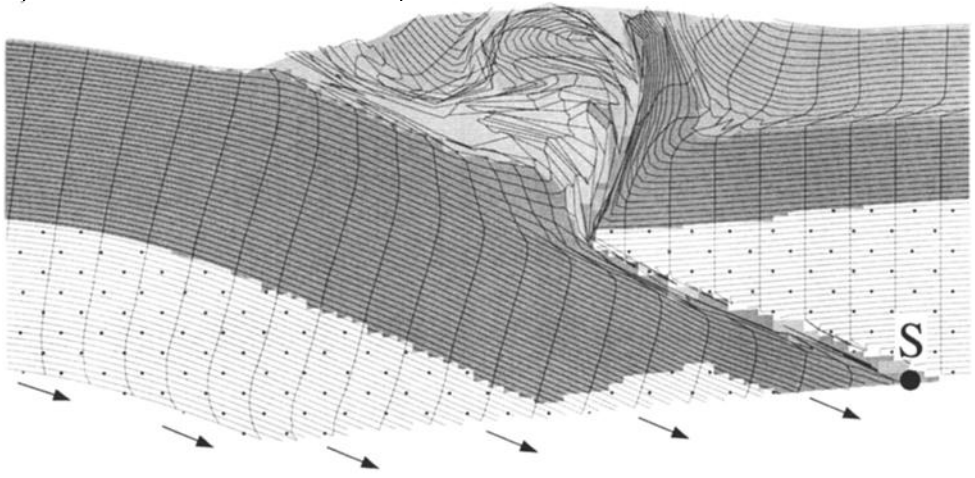

f) Deformation and Materials, Δx = 300 km

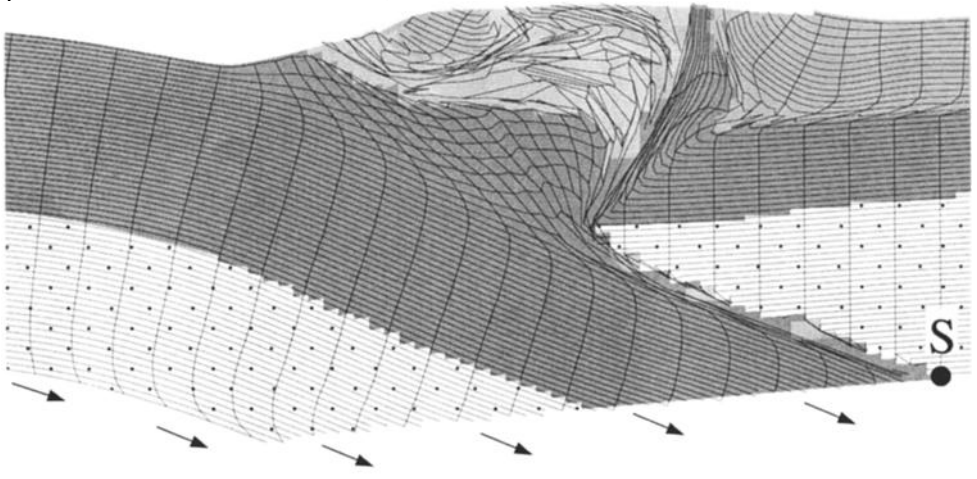

Figure 12. (continued.)

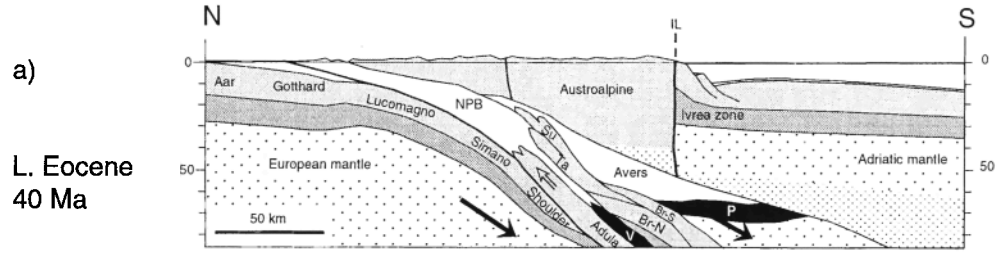
a)
L. Eocene
40 Ma
onset of collision (after 555 km of convergence)
N
S
IL
Aar
Gotthard
Lucomagno
NPB
Austroalpine
Ivrea zone
Sm
Ta
Avers
Simano
Shoulder
Adula
Br-S
Br-N
P
European mantle
Adriatic mantle
50 km
0
50

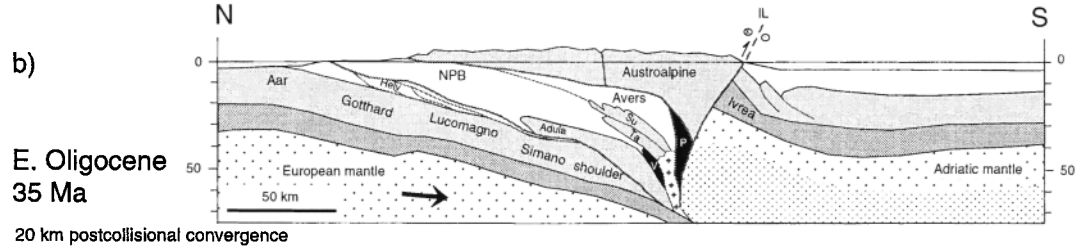
b)
E. Oligocene
35 Ma
20 km postcollisional convergence
N
S
IL
Aar
Helv
NPB
Austroalpine
Avers
Gotthard
Lucomagno
Adula
Simano shoulder
Ivrea
European mantle
Adriatic mantle
50 km
0
50

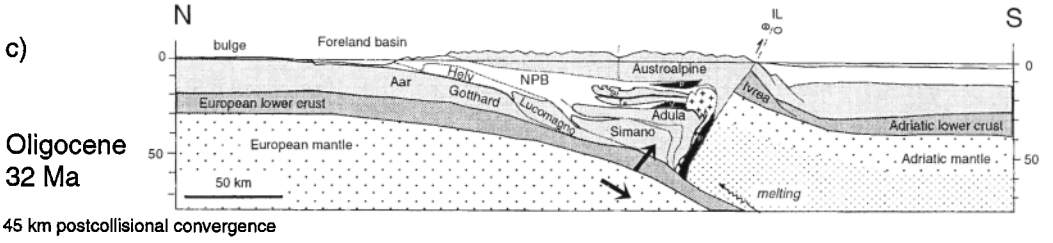
c)
Oligocene
32 Ma
45 km postcollisional convergence
N
S
IL
bulge
Foreland basin
Helv
NPB
Aar
Austroalpine
Gotthard
Lucomagno
Ivrea
European lower crust
Adula
Simano
Adriatic lower crust
European mantle
Adriatic mantle
50 km
melting
0
50

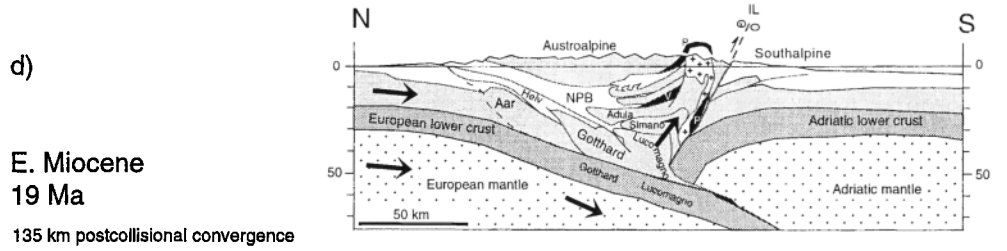
d)
E. Miocene
19 Ma
135 km postcollisional convergence
N
S
IL
Austroalpine
Southalpine
Aar
Helv
NPB
Adula
Simano
Gotthard
Lucomagno
European lower crust
Adriatic lower crust
European mantle
Adriatic mantle
50 km
0
50

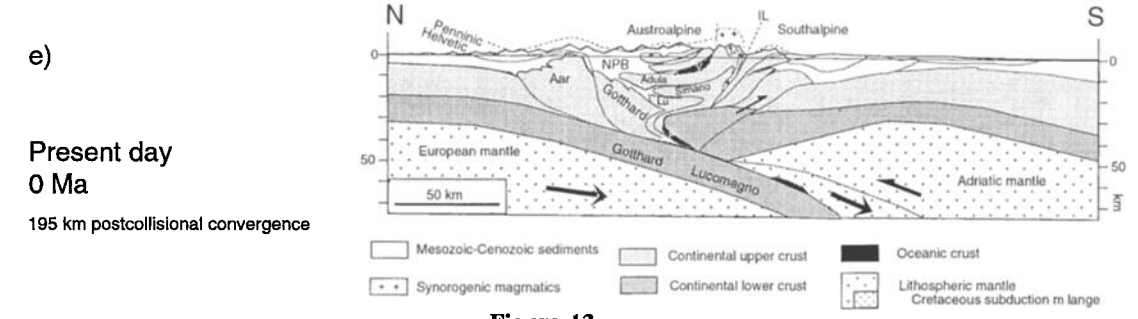
e)
Present day
0 Ma
195 km postcollisional convergence
N
S
IL
Penninic
Helvetic
Austroalpine
Southalpine
NPB
Aar
Adula
Simano
Lu
Gotthard
European mantle
Lucomagno
Adriatic mantle
50 km
0
50
km
Mesozoic-Cenozoic sediments
Continental upper crust
Oceanic crust
Synorogenic magmatics
Continental lower crust
Lithospheric mantle
Cretaceous subduction m lange

Figure 13.

sections were constructed for the transect through eastern Switzerland. The individual reconstructions show typical situations and correspond to moments in the evolution which are suitably constrained by geologic data.

The retrodeformed cross sections were constructed by using estimates of length and thickness of various tectonic units, constrained by structural arguments, estimates of depth derived from petrologic, structural, and geochronological data; stratigraphic-sedimentological data, and other boundary conditions, including strike-slip motions in and out of the section plane. A similar set of reconstructions is presented by *Schmid et al.* [1996, 1997a, 1997b], who also provide an in-depth discussion of the data constraining the reconstructions.

4.1. Incipient Collision of Continental Crust

The inferred geometry of the subduction zone in Eocene times, after the Valais trough had closed, is displayed in Figure 13 a [see also *Schmid et al.*, 1997 a, 1997b, 1996]. Continued convergence led to the collision of the Adriatic and European margins. The ensuing collision processes will be now discussed in more detail.

Assuming pressures were close to lithostatic, the tip of the European margin was subducted to a peak depth of ~80 km as indicated by peak pressures of 27 kbar and syneclogitic penetrative deformation at 42-37 Ma. The upper crustal rocks pertaining to this tip are preserved in the southern part of the Adula nappe. These rocks subsequently experienced isothermal decompression, interpreted to represent exhumation by forced extrusion [*Escher and Beaumont*, 1997; *Schmid et al.* , 1997a, 1997b]. The trailing part of the Adula upper crustal unit, the unit marked "shoulder" between Adula and Simano in Figure 13a, is inferred to be a basement high from paleogeographic reconstruction of the Mesozoic sediments deposited on this margin. However, the "shoulder" cannot be associated with any of the basement units observed at the surface. This missing upper crustal unit is assumed to have been subducted.

The sedimentary cover of Adula and "shoulder" basement was stripped off from its substratum and now forms the stack of cover nappes represented in the North-Penninic Bündnerschiefer (NPB in Figure 13a). Generally speaking, growth of the wedge occurred by episodic imbrication and by sequential detachment: the cover sediments were detached first and remained at a shallower position, while the upper crustal crystalline basement moved further down the subduction conduit before being detached. This process gave rise to two largely independent nappe stacks.

By 35 Ma, rapid exhumation, attributed by most authors to be by forced extrusion, had placed the northern part of the Adula nappe to a level corresponding to pressures of 6-8 kbar within the Penninic nappe stack. The emplacement of the Adula nappe was followed by the intrusion of the Bergell granodiorite at the rear of the Adula nappe in Early Oligocene times. Geochemical signatures suggest a contribution of mantle material to the melts of this intrusion. *von Blanckenburg et al.* [1998] suggested slab break off of the subducting plate and subsequent mantle upwelling to provide such a mantle source, an idea taken up in the reconstructions of *Schmid et al.* [1996, 1997b]. Alternatively, it could be argued that the subduction of young and hot lithosphere underlying the Piemont ocean and the Valais trough provided the heat and fluids to generate the melts in the overlying mantle (V. Trommsdorff, oral communication, 1999).

As shown in Figure 13b, the sedimentary cover of the Lucomagno and Gotthard upper crustal units were scraped off at this stage. These cover sediments now form the south Helvetic nappes, a highly allochthonous nappe stack detached from its crystalline basement.

Figure 13b also shows the base of the Austroalpine nappes, taken as a marker horizon, starting to deform into a south vergent antiform. This backfolding or retroshearing marks the onset of backthrusting and strike-slip motion along the Insubric Line, predating the final emplacement of the Bergell intrusives. Farther east, south vergent thrusting affected the Southalpine units. However, the section south of the Insubric Line, as shown in Figure 13b, containing the Ivrea lower crustal and mantle section, lacks such thrusting. It corresponds to a section that is at present situated farther west due to subsequent dextral strike slip movement along the Insubric Line.

4.2. Underplating of Continental Crust, Retrothrusting and Erosion

By 32 Ma the melts of the Bergell intrusion were rising (tonalite part) and cooling (granodiorite part) along the retroshear zone of the Insubric Line. This fault zone was active as retro-thrust as well as dextral strike slip fault, and it is conceivable that deformation along it provided the channels for the melts to rise.

Offscraping of continental upper crust continued in more external positions (Lucomagno and Simano units). Subduction of lower crust continued. The coeval formation of an upper crustal nappe pile, subduction of the associated lower crust,

Figure 13. (opposite) Retrodeformed cross section along the eastern traverse of the Swiss Alps for five time slices. The cross sections are aligned approximately along the Insubric Line (IL). Helv, Helvetic nappes; NPB, North-Penninic Bündnerschiefer; P, V, Piemont and Valais oceanic crust. (a) Late Eocene (40 Ma) stage showing incipient collision and forced extrusion of subducted European margin (Adula thrust sheet). Abbreviations are as follows: for underplated upper crustal units of Briançonnais microcontinent, Su is for Suretta, Ta is for Tambo; for subducted Briançonnais microcontinent, Br-S is for leading margin, Br-N is for trailing margin. (b) Early Oligocene (35 Ma) stage showing onset of backfolding and retrothrusting. (c) Oligocene (32 Ma) stage showing underplated European upper crust (Simano, Adula thrust sheets), continued backfolding (arrow) and retrothrusting along Insubric Line (IL), and onset of exhumation of Austroalpine nappes. (d) Early Miocene (19 Ma) stage showing continued backfolding and retrothrusting and exhumation of Penninic nappes. (e) Present-day structure (0 Ma). The Insubric Line (IL) is shunted across Adriatic lower crust and deformation of the Adriatic crust has led to a bivergent orogen. Lu, Lucomagno basement block.

and retrothrusting led to underplating of upper crustal units associated with backfolding, a typical association for Alpine structures north of the Insubric Line. Erosion must have set in rapidly because only 4 Ma later, boulders of Bergell granodiorite appeared in the clastic sequence of the Gonfolite Lombarda south of the Insubric Line.

In cross-sectional view, exhumation of the Penninic-Austroalpine block occurred by plug uplift (P-U mode of *Beaumont et al.* [1999]) with a pro-wedge developing from the growing Penninic nappe pile and a major retro-thrust, the Insubric Line. In addition, out of plane movements occurred at this time. E-W extension near the base of the Austroalpine nappes is recorded by the Turba normal fault, a fault that is truncated by the Bergell intrusion. Dextral motion along the Insubric Line persisted, contributing to the change of lithosphere section discussed earlier. At this stage the Adriatic section along this transect most probably still had a south dipping crust-mantle boundary. The Ivrea body, a cold mantle piece remnant of Jurassic rifting [*Handy et al.*, 1999] may have acted much like a rigid backstop, sheltering the Southalpine crust from incorporation into a retro-wedge. As shown in Figure 13c, the cover sediments of the Gotthard and adjacent units to the north were detaching from their crystalline basement, later forming the Helvetic nappes.

4.3. Exhumation of Penninic Block (More Retrothrusting and Erosion)

A comparison of Figures 13c and 13d show that during this time interval, offscraping of upper crust by pro-thrusting propagated to the north coeval with south vergent retrothrusting along the Insubric Line, which exhumed the Bergell intrusion and adjacent units to the north. Retrothrusting along the steeply dipping Insubric Line was more rapid than pro-thrusting along the gently dipping pro-thrust. As a consequence, the base of the Austroalpine block and the underlying suture of the former Piemont ocean experienced a rotation in this time interval, changing from an initially southern dip to a northern dip.

The lower crust of the European margin continued to be subducted. The offscraped upper crust was advected and accreted to the hanging wall in front of the tip of the Adriatic lower crust (Figure 13d). This accretion process was responsible for large scale backfolding of the various units, steepening the southern limbs into parallelism with the Insubric Line (Southern Steep Belt of *Milnes* [1974]); the process is dubbed "postnappe folding" in the Alpine literature.

The growth of the pro-wedge is illustrated by the Helvetic nappes which travelled north, overriding the internal basin fill of the north Alpine foreland basin. The pro-wedge underwent E-W extension, which is indicated by low-angle normal faulting within the Penninic nappes (Forcola fault [cf *Baudin et al.*, 1993]).

Dextral strike slip along the Insubric Line continuously replaced the Southalpine lithosphere section, so that by 19 Ma the crust-mantle boundary was north dipping. As shown in Figure 13d, incipient south vergent thrusting occurred within the upper crust of this section.

4.4. Shunting/Indentation and Bivergent Thrusting

The Southalpine nappe stack depicted in Figure 13e (present-day structure) evolved mainly in poste-early Miocene times. It includes detachment and stacking of cover nappes as well as stacking of upper crust scraped off its lower crust. The deformation propagated in a southerly direction, leading to the formation of a retro-wedge. Comparing Figures 13d and 13e, it follows that this retro–wedge widened from a retroshear zone involving essentially the Insubric Line to the formation of a thick-skinned fold-and-thrust belt. As pointed out earlier, the detachment horizon at midcrustal level was now dipping north, an orientation possibly more favorable to detachment in the growing retro-wedge than the geometry prevailing earlier (Figure 13c) with a south dipping Moho.

In the pro-wedge north directed stacking of European upper crust continued and included the uplift of the Aar massif and the associated Subalpine Molasse nappe stack. Farther to the west, thrusting propagated far out into the foreland to form the Jura Mountains. Thus the Alps were characterized by bivergent thrusting in this time period.

The lower crust of the European margin has been interpreted to underlie the mantle of the Adriatic margin from seismic refraction and reflection data, with a geometry as shown in Figure 13e [cf. *Ye*, 1992; *Pfiffner and Hitz*, 1997; *Schmid et al.*, 1996, 1997a, 1997b]. The upper boundary of the Adriatic lower crustal wedge is in a higher position beneath the Insubric Line compared to farther south. This is interpreted as south vergent lower crustal imbrication in Figure 13e and may be linked to upper crustal imbrication. Generally speaking, the upper crust of both the European and the Adriatic margins are involved in bivergent imbrications above the asymmetric subduction geometry of the lower crustal and lithospheric mantle structure.

Detachment and south vergent thrusting of the upper crust of the Adriatic margin resulted in juxtaposition of Adriatic lower crust and European upper crust. The latter was displaced southward across the Adriatic lower crust, a process referred to here as "shunting". This "shunting" was possibly facilitated by the north dipping Adriatic crust and mantle, which placed a potential detachment horizon (e.g., base of upper crust) into a more favorable position. The tip of the Adriatic lower crustal wedge represented a "singularity point" for south directed material flux: material arriving above the tip was shunted across the wedge and contributed to the buildup of the retro-wedge, whereas material arriving beneath the tip was subducted into the mantle. Relative to the incoming or pro-crust, the "singularity point" was situated at midcrustal levels and the situation can be described as divergent flow. Considering the retroside, on the other hand, the kinematics can be described in terms of "wedging" or "indentation".

5. Discussion: Comparison Between Numerical Experiments and the Swiss Alps

The Alps are a complex, multiphase orogen with many variations in properties and structure along and across strike.

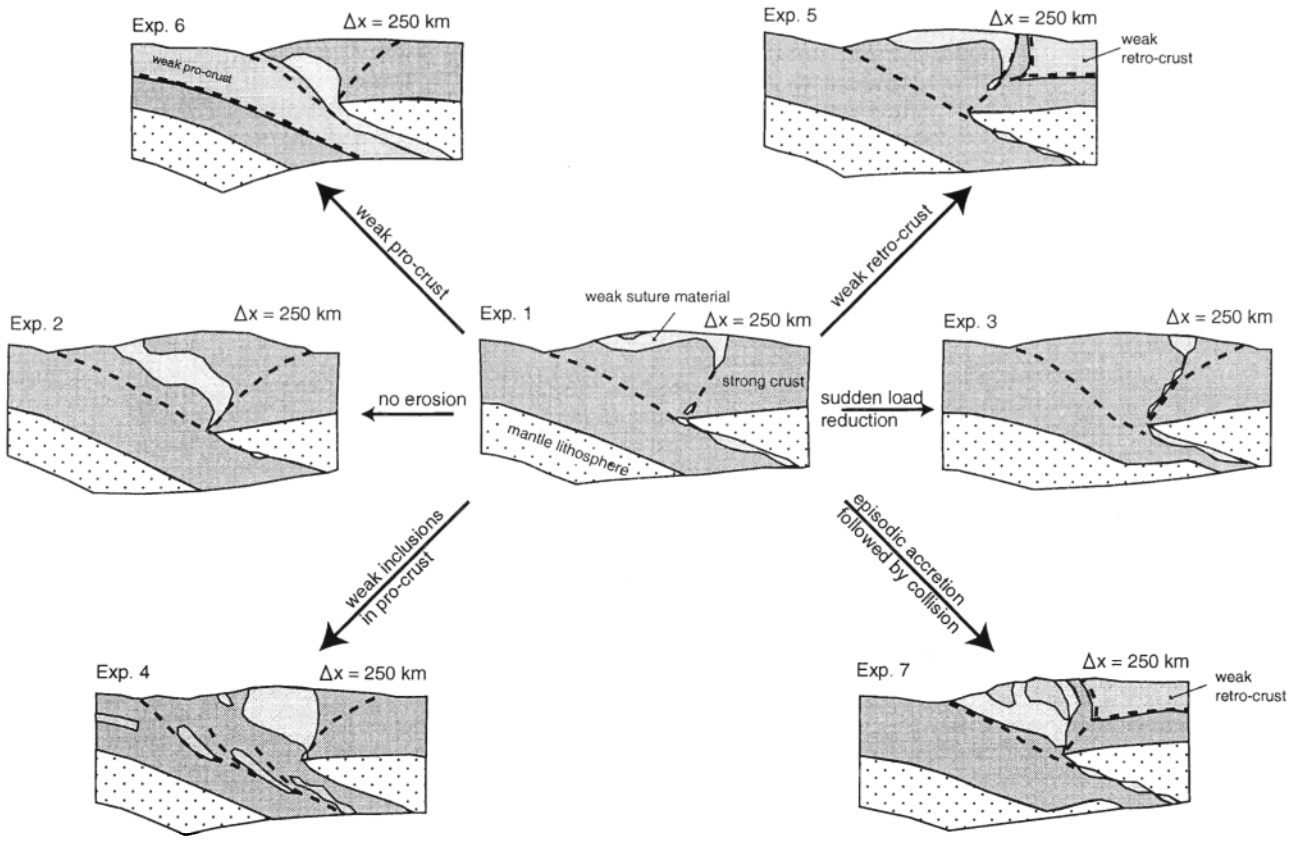

Figure 14. Composite diagram showing crustal structures obtained from dynamic modeling after 250 km of convergence (indicated at top right of each panel). E1 is shown in the center, surrounded by variations. Main distinctions from E1 are indicated along the arrows. Light gray shading indicates weak suture material, medium gray shading indicates weak upper crust, and dark gray shading indicates strong continental crust. (top) Experiments including weak upper crust in lower or upper model plate, (middle) experiments with strong upper crust for varying erosion rates/subduction loading, and (bottom) more complex models displaying lateral heterogeneities within pro-crust.

There is no intent to use the simple numerical experiments to reproduce or simulate Alpine dynamics directly. Instead, comparisons with the Alpine reconstructions can be used to infer what may have been the first-order controls on Alpine orogenesis and, by extension, orogenesis in general. The first-order characteristics described below denote each subtopic by a plus when some or all of the model experiments predict Alpine-type behavior and a minus for those Alpine features that cannot be addressed by any of the model experiments. For ease of comparison, we have summarized the main results from the model experiments into a schematic figure (Figure 14).

5.1. Crustal Thickness, Convergence Amounts and Exhumation of Suture Material (+)

To be consistent with the paleostructure of the Alps based on geologic and petrologic data, the model experiments must predict similar amounts of convergence and crustal thickening. The amount of convergence necessary to backthrust, uplift, and exhume material from the subduction complex depends primarily on the rate of erosion, the percentage of incoming flux that is subducted, and the distribution of uplift and exhumation across strike. In models with moderate erosion rates and homogeneous strong pro-crust (e.g., E1 and E5), suture material is exhumed after ~200-250 km of convergence (Figure 14). Suture exhumation does not take place synchronously across strike but varies with location as a result of uneven uplift and exhumation patterns (see section 5.2). Maximum crustal thicknesses are of the order of ~70 km after 200 km of convergence. In these respects, E1 and E5 are similar to Alpine estimates. For example, according to the reconstruction for the eastern Swiss traverse, suture material (the upper Penninic nappe stack) is located at the surface after ~200 km of convergence since the onset of collision in Oligocene times, and maximum crustal thickness is presently ~65 km.

Other model experiments do not develop Alpine-type dimensions and geometry (Figure 14). E2 (with no erosion) fails to exhume suture material to the surface, but the model serves as a good "control" to illustrate the difference when erosion is not significant. It also shows exhumation of ~10

km of suture material owing to extensional thinning of the overlying crust (Figure 7b beneath the topographic maximum). E3, with a sudden decrease in subduction load L, predicts ~65 km maximum crustal thickness but exhumes suture material in its original retrodipping geometry. E4 and E6 shift the locus of deformation proward using weak detachment horizons, changing the flexural loading of the model orogen and, as a result, its geometry and flux imbalance. In the case of E4, this merely delays the exhumation of suture material, but E6 ceases uplifting and exhuming material altogether, resulting in complete continental subduction. Such a situation is not observed in nature and suggests that wholescale pro-crustal detachment is unlikely. The most complex model, E7, includes an extra subduction-accretion phase prior to collision, has a thicker suture package, and experiences some uplift and exhumation prior to the onset of collision. In comparison to the eastern Swiss traverse, this experiment exhumes suture material too early. However, similar nappe accretion experiments that have a small component of subduction zone retreat allow nappes to be accreted without experiencing early uplift and exhumation [*Ellis et al.*, 1999].

5.2. Erosion Rates (+)

Application of a simple model in which erosion rate is proportional to topographic height produces an asymmetric model exhumation pattern with uplift and erosion rates increasing in the back (retro)direction. Erosion in these models only becomes active after uplift forms positive topography. A first-order comparison between erosion rates in the models and those estimated for the Swiss Alps can be made using simple mass balance arguments for model experiments. In E1 the decrease in subduction flux F_2 to 80% of incoming flux F_1 during the transition to collision is eventually balanced by a corresponding erosion flux (20% F_1) giving a steadystate topography (Figures 5d-5f). The average denudation rate in this case is $0.2F_1/W$, where W is the width of the orogen (~80 km), giving a rate of 1.5 mm/yr^{-1} (i.e., 15 km of denudation per 100 km convergence). The maximum denudation rate estimated from velocity vectors (Figure 6c) is about twice the average rate, or 3 mm/ yr^{-1}, giving 30 km erosion per 100 km convergence. The other experiments with moderate erosion rates and continued uplift of the orogen give similar results.

In the Alps, erosion rates were variable in time and space. Erosion rates were highest close to the Insubric Line (the retroshear zone) and much lower in the external zones of the orogen. *Schlunegger and Willett* [2000] estimated denudation rates based on cooling histories to be of the order of 0.3-1 mm/yr^{-1}. Glacial and postglacial erosion rates determined from Pleistocene gravel terracess [*Graf*, 1993] and filling of glacially overdeepened Alpine valleys [*Pfiffner et al.*, 1997] give values of 0.3-5 mm/yr^{-1} which compares with present-day erosion rates (0.5 mm/yr^{-1}) determined from the growth of river deltas into peri-Alpine lakes [*Jäckli*, 1958] and with the values associated with the experiments shown here.

5.3. Onset of Backthrusting and Bivergent Thrusting Pattern (+)

The model experiments with strong, uniform crust (E1-E3) all develop a bivergent geometry during the transition from subduction to collision (between 0 and 50 km of convergence). The bivergence results from two oppositely verging shear zones which originate from the tip of retro-mantle lithosphere, marking the separation point between material which passes into the uplifting region and that which is subducted. The retroshear zone (or backthrust in terms of predominant flow geometry) remains focused within strong retro-crust as convergence continues.

The dynamics and strength of the retroshear zone that develops depend on the exact model configuration. For example, E3 experiences a large increase in uplift and retroshearing during the sudden reduction in subduction load between 50 and 58 km convergence. Retroshearing and the uplift of suture material do not continue in E2 (which has no erosion) or E6 (where deformation propagates proward and flexural loading reopens the subduction exit region). Model experiments with a weak retro-upper crust (E5 and E7, Figure 14) also develop bivergent geometry, but detachable retro-crust allows deformation to propagate retroward, as discussed in section 5.6. As a consequence, a much wider retro-wedge develops, a situation comparable to the geometry of the Southern Alps in the eastern Swiss traverse.

The onset of retroshearing during entrance of pro-continental crust is in agreement with reconstructions from the eastern Swiss traverse, where the entrance of European continental lithosphere into the subduction zone (and possibly slab break off) at ca. 40-35 Ma triggered a transition from single-vergent subduction to bivergent orogenesis. This transition coincided with backthrusting of the Peninnic nappe stack along the Insubric Line.

5.4. Formation of Basement Nappes (+)

In the Alps, northward propagation of pro-deformation occurred by discrete shearing along a series of basement thrusts, e.g., as is currently observed along on the northern sides of the Aar and Gotthard basement blocks. Earlier localized pro-shearing led to the formation and underplating of a series of basement nappes (the lower Penninic nappe stack) at ca. 32 Ma. The development of discrete shear zones and associated basement nappes has been attributed to pre-Alpine heterogeneities within the European basement [*Pfiffner et al.*, 1990].

Model experiments also suggest that pretectonic or syntectonic zones of weakness influence the formation of basement nappe stacks and/or massifs. The model experiments that have a homogeneous strong pro-crust (E1-E3 and E5) do not develop discrete thrust-sense shear zones. Only E4, which has a series of material heterogeneities causing strength differences (here simplified to a series of rectangular inclusions), shows focused thrusting along a series of pro-stepping shear zones and associated crustal-scale folding (Figure 14). Compared to E1, E4 has reduced amounts of plug exhumation because the locus of thickening is transferred proward within the basement uplifts. The weak inclusions are eventually subducted but leave behind a complex pro-wedge deformation pattern. Similar experiments (not shown) demonstrate that when the weak inclusions are closer together than those shown in E4, their basal detachments couple together laterally through the intervening strong parts at the crust, leading to a style similar to E6.

A more complex case, E7, shows how material heterogeneities can lead to large-scale fold nappes encased in sedimentary suture material. Such structures form in response to the initial geometry (a microcontinent between two model oceans) and are analogous to the Monte Rosa nappe of the Swiss-Italian Alps.

Inherited weaknesses may not be the only cause for discrete jumps in pro-deformation and basement thrusts/fold nappes. Syncollisional strain weakening leading to shear localization (e.g., caused by changes in deformation mechanisms [*Guermani and Pennacchioni*, 1998; *Herwegh et al.*, 1999] or thermal evolution [e.g., *van den Beukel*, 1992] may produce similar deformation patterns. In this case, the spacing of discrete pro-thrusts is controlled by dynamic processes rather than resulting from inherited margin geometry.

5.5. Rotation and Deformation of Suture Material (+)

According to the reconstructions, the upper Penninic nappe stack in the Alps has experienced a rotation from an original south dipping geometry to near horizontal or north dipping (Figure 13). The model experiments illustrate two possible mechanisms by which such a rotation may occur: (1) by focusing of pro-shear within weak suture material at the onset of collision and (2) by focusing of retroshear, giving rise to an asymmetrical erosion pattern that enhances exhumation near the model backthrust. In E1, E5, and E7 the combined effect is enough to rotate the suture zone from retro-dipping to pro-dipping during ca. 250 km of convergence (Figure 14). This rotation is accompanied by early shearing in the suture zone (e.g., Figures 10a and 10b). Later, the suture material is advected passively and experiences little further deformation. An equivalent experiment (not shown here) in which the suture material has the same properties as the rest of the crust, shows no rotation of the suture during exhumation.

The erosion-driven rotation seen in the experiments is model-dependant in that erosion depends on elevation, which in turn depends on internal crustal dynamics. However, as discussed in section 5.2, asymmetric exhumation is also observed for the Alps. If model experiments capture some of the first-order dynamics of an Alpine-type orogen, they suggest that erosion may be an important factor in promoting rotation of suture material to a horizontal attitude at the surface.

Other factors not investigated here may also promote rotation of material within the uplifting orogenic core. Any effect which weakens the strength of the retroshear zone will increase the amount of plug rotation [e.g., *Niño et al.*, 1998]. Weakening may result from fluid infiltration, strain softening, and/or thermal effects associated with the intrusion of magma. For example, in the Alps intrusion of the Bergell pluton occurred at ca. 32 Ma along the Insubric Line, about the same time as backthrusting along this shear zone initiated [*Schmid et al.*, 1997a, 1997b]) and the interdependence of magma intrusion and motion along this fault has been discussed by a number of workers [*Berger et al.*, 1996; *von Blanckenburg et al.*, 1998; *Laubscher*, 1983; *Pfiffner*, 1992; *Rosenberg et al.*, 1995].

Models that do not experience rotation of suture material also provide some insight into this process and the factors that will suppress it (Figure 14). For example, a sudden reduction in subduction load (E3) prevents early rotation of the suture by changing collision geometry, moving the suture more rapidly retroward and exposing the whole uplifted plug above baselevel, which causes a more symmetric erosion pattern to develop (e.g., Figure 9e, which shows velocities for steadystate topography). In E4 the initial rotation occurs, but later plug uplift and rotation are suppressed by the outward stepping of deformation and uplift within the heterogeneous basement nappes on the proside. Models in which uplift and exhumation cease early on (E2 and E6) also do not experience suture rotation, although in these cases the suture material continues to shear and deform throughout the experiment.

5.6. Shunting of Collision Zone over Retro-Crust (+)

The later stages of evolution of the eastern Swiss Alps involved the formation of a retro-wedge and the propagation of deformation and thickening southward (Figures 2a and 2b and 13d). Two model experiments show a similar effect as a result of a weak ductile horizon within the retro-crust (E5 and E7, Figure 14). In these cases, the ductile horizon acts as a detachment and allows retroward propagation of deformation once sufficient topography has been formed (after ~50-100 km postcollisional convergence, Figure 10). The retroshear zone emanating from the mantle lithosphere wedge is eventually directly linked to the midcrustal detachment horizon (Figures 10d and 10e). As a consequence, material is moved retroward along a gently dipping shear zone, the process that we call shunting.

These models illustrate the role of mid-crustal or lower-crustal detachments in allowing deformation to propagate away from the core of an orogen. The homogeneous properties of retro-upper crust in the experiments preclude the formation and stacking of a thick-skinned fold-and-thrust belt, but such features would also be likely if heterogeneities and/or synconvergent strain localization effects were present (see E4 and section 5.4).

In E5 and E7 the location of maximum finite shear and deformation at the surface is a function of the amount of convergence. For small amounts of collisional convergence (e.g., Figures 10a-10c), no strong shear zone is visible at the surface. Later, shunting of the uplifted lower crustal segment over the retro-crust leads to exposure of two shear zones: a steeper one located within the weak suture material next to the lower crustal body and a second, shallower dipping zone between the lower crustal body and the upper crustal synform. At depth these two shear zones gradually merge.

The model observations outlined above, with the exception of the synform, suggest that interpretation of the steeply dipping Insubric Line in terms of a single retroshear zone (e.g., section 5.3) may be an oversimplification. Instead, retroshearing may have changed position along and across strike during evolution of the collision zone. This speculation is in agreement with observations from the Alps, where the location of maximum shear as indicated by the mylonite zone along the Insubric Line was not the location of active shearing in the later stages of collision when the Southern Alps were imbricated.

5.7. Exhumation of Lower Crust (+) and Change in Collision Geometry Along Strike (-)

In the Swiss Alps the change in geometry of the Adriatic plate along strike appears to have exerted a first-order control on the style of the orogen [*Stampfli and Marchant,* 1997]. In particular, the change in dip of Adriatic lower crust (from south dipping at the western end to north dipping at the eastern end) [*Waldhauser et al.,* 1998; *Schmid et al.,* 1997b] is correlated with a change in the amount of shortening; shortening increases from the transect through the central to eastern Swiss Alps (Figure 2), and it further increases to the east [*Schönborn,* 1992]. The change in configuration of Adriatic lower crust along strike may result from the original rift geometry of the margin [*Schmid et al.,* 1987, 1989; *Handy et al.,* 1999]. We speculate, however, that this process may have been augmented by later collisional dynamics, as explained below.

E5 and E7 show how retro-lower crust may be uplifted and exhumed during collision (Figure 14). The retroshear zone emanating from the tip of the retro-mantle connects to the base of the weak retro-upper crust and produces an uplifted triangular-shaped piece of lower crust similar to the one observed in the central traverse (Ivrea zone in Figure 2a). The similarity with model experiments suggests that the Ivrea zone may have been tilted and exhumed during collision as a result of backthrusting. However, in the eastern traverse (Figure 2b), no such uplifted lower crustal piece is observed. The lack of lower crustal uplift in the eastern traverse may indicate that the lower crust now present in this transect was situated deeper and farther retroward of the S point than in the model experiment configurations and thus avoided retro-transport and uplift, while the already uplifted rift flank farther west in the Alps underwent further uplift. There are other possible explanations for the discrepancy, including (1) a variation in lower crustal strength along strike, with stronger lower crust in the east which resisted retroshearing, so that shear focused around a nose of lower crustal material and did not uplift it (Figure 13e), and (2) weaker lower crust thickened by distributed shear and detached from underlying lithospheric mantle. These two alternative explanations require a spatially varying lower crustal rheology, particularly a difference between European and Adriatic lower crust.

Farther to the west the uplifted nose of mantle lithosphere and lower crust (the Ivrea Body and Ivrea Zone) do not appear to have been extensively deformed during collision but probably reflect the initial (rift) geometry. Their presence appears to have controlled orogenic thickening, which could not propagate southward through the strong, deformation-resistant lower lithosphere, thereby creating a geometry more like E1.

5.8. Extensional Exhumation Above Plug Across (+) and Along (-) Strike

Uplift of crust that contains weak detachment horizons within it can cause extension in overlying crustal material [*Willett,* 1999]. This effect is observed in E5 and E7, where the weak ductile horizon at midcrustal levels within retro-lithosphere causes extension in the overlying, relatively undeformed hangingwall material (Figure 10c). Extension of up to 150% is observed in E5 and causes a significant amount of exhumation in addition to that caused by erosion

Synorogenic extension has been suggested for the Austroalpine nappes [*Froitzheim et al.,* 1994]. This orogen-parallel extension affected the top 5 km and is held partially responsible for exhumation of the Lepontine high-grade rocks by oppositely facing low-angle normal faults (Simplon fault to the west [*Mancktelow,* 1992], and Turba and Forcola faults to the east [cf. *Nievergelt,* 1996, *Baudin,* 1993]). Given the few normal faults recognized and their moderate heaves, only a few kilometers of exhumation can be attributed to these faults. That the current models predict extension parallel to convergence is a strong indicator that in equivalent three-dimensional models, extension would be even more pronounced parallel to the strike of the orogen.

6. Conclusions

This study compared kinematics of Alpine evolution as derived from series of retrodeformed cross sections (based on structural and other geologic data) and forward modeling (subduction-collision experiments using numerical models) in order to gain insight into Alpine dynamics. Retrodeformation shows that Cenozoic collision between the European and Adriatic margins involved underplating of European continental crust, which was later exhumed by backthrusting and concurrent denudation. During the last phase of collision, European upper crust in the eastern Swiss Alps was shunted southward over Adriatic lower crust. The Adriatic upper crust was peeled off in this process and stacked southward to form a nappe pile. The result was a bivergent orogen above an asymmetric subduction zone.

For a reasonable set of material, kinematic, and erosion parameters the forward models are in first-order agreement with mass balance predictions from retrodeformed cross sections. Comparison between these sections and some of the more Alpine-type model experiments and, particularly with the final model (E7) show the following points of agreement: (1) collision of model continents following subduction results in crustal thickening and leads to similar values of crustal thicknesses to those observed in the Swiss Alps, (2) for moderate model erosion rates the amounts of exhumation and spatial variation of exhumation strongly resemble the pattern exposed in the Swiss Alps, (3) models and reconstructions both predict onset of retroshear (backthrusting) during entry of pro-continental crust, (4) basement nappes can be formed by focusing of shear along heterogeneities representing pre-Alpine structures, (5) rotation of the suture to a near-horizontal attitude results from erosion and focusing of retroshear (backthrusting), and (6) shunting of pro-upper crust retroward occurs when detachable retro-upper crust is present. By shunting we mean that material from the uplifted plug moves retroward on a gently dipping detachment over the retro-lithosphere.

E7 also shows how a precursor episode of accretion leads to formation and stacking of a crustal fold nappe in the subduction zone and how it will be incorporated into subsequent collision. Finally, the presence of an uplifted piece of lower crust in E5 and E7 suggests that exhumation of the Ivrea lower crustal body may have partially resulted from collisional dynamics.

Despite these broad points of agreement, there are also many discrepancies between model experiments and structures derived from the Alpine orogen. Future studies require models to incorporate three-dimensional effects, thermal evolution, behavior of mantle lithosphere in a more dynamical way, and more realistic rheological behaviors.

Acknowledgments. Research was funded by Swiss National Foundation grant 20-43246.95 to A.P. and Lithoprobe Supporting Geoscience and NSERC research grants to C.B. C.B. also acknowledges funding through the Inco Fellowship of the Canadian Institute for Advanced Research. Comments from Reini Zoetemeijer, Carlo Doglioni, and François Roure improved the manuscript. Lithoprobe contribution number 1172.

References

Axen, G., J. Selverstone, T. Byrne, and J. Fletcher, If the strong crust leads, will the weak crust follow?, *Geol. Soc. Am. Today, 8*, 1-8, 1998.

Baudin T., D. Marquer, and F Persoz, Basement-cover relationships in the Tambo nappe (Central Alps, Switzerland). Geometry, structure and kinematics, *J. Struct Geol., 15*(3-5), 543-553, 1993.

Beaumont, C., P. Fullsack, and J Hamilton, Style of crustal deformation caused by subduction of the underlying mantle, *Tectonophysics, 232*, 119-132, 1994.

Beaumont, C., S. Ellis, J. Hamilton, and P. Fullsack, Mechanical model for subduction-collision tectonics of alpine-type compressional orogens, *Geology, 24*, 657-678, 1996.

Beaumont, C., S. Ellis, and O A. Pfiffner, Dynamics of sediment subduction-accretion at convergent margins: Short-term modes, long-term deformation, and tectonic implications, *J. Geophys. Res., 104*, 17,573-17, 601, 1999.

Berger, A., C. Rosenberg, and S.M. Schmid, Ascent, emplacement and exhumation of the Bergell pluton within the Southern Steep Belt of the Central Alps, *Schweiz. Mineral. Petrogr. Mitt., 76*, 357-382, 1996.

Boland, J.N., and T.E. Tullis, Deformation behaviour of "wet" and dry clinopyroxene in the brittle to ductile transition region, in *Mineral and Rock Deformation: Laboratory Studies, Geophys. Monogr. Ser., vol. 36*, edited by B.E. Hobbs and H.C Heard, pp. 35-50, AGU, Washington, D.C., 1986.

Bousquet, R., B. Goffé, P. Henry, X. Le Pichon, and C. Chopin, Kinematic, thermal and petrological models of the Central Alps; Lepontine metamorphism in the upper crust and eclogitisation of the lower crust, *Tectonophysics, 273*, 105-127, 1997.

Carter, N.L., and M.C. Tsenn, Flow properties of continental lithosphere, *Tectonophysics, 136*, 27-63, 1987.

Chopin, C., Coesite and pure pyrope in high-grade blue-schists of the Western Alps. A first record and some consequences, *Contrib. Mineral. Petrol., 86*, 107-118, 1984.

Chopra, P.N., and M.S. Paterson, The role of water in the deformation of dunite, *J. Geophys. Res., 89*, 7861-7876, 1984

Davies, J.H., and F. von Blanckenburg, Slab break off: A model of lithosphere detachment and its test in the magmatism and deformation of collisional orogens, *Earth Planet. Sci. Lett., 129*, 85-102, 1995.

Davis, D., J. Suppe, and F A Dahlen, Mechanics of fold-and-thrust belts and accretionary wedges, *J. Geophys. Res., 88*, 1153-1172, 1983.

Doglioni, C., and A. Bosselini, Eoalpine and Mesoalpine tectonics in the Southern Alps, *Geol. Rundsch., 76*(3), 735-754, 1987.

Ellis, S., C. Beaumont, and O.A. Pfiffner, Geodynamic models of crustal-scale episodic tectonic accretion and underplating in subduction zones, *J. Geophys. Res., 104*, 15,169-15,190, 1999

Escher, A , and C. Beaumont, Formation, burial and exhumation of basement nappes at crustal scale: A geometric model based on the western Swiss-Italian Alps, *J. Struct. Geol., 19*(7), 955-974, 1997

Froitzheim, N., S.M. Schmid, and P. Conti, Repeated change from crustal shortening to orogen-parallel extension in the Austroalpine units of Graubünden, *Eclogae Geol. Helv. 8*(2), 559-612, 1994.

Fullsack, P., An arbitrary Lagrangian-Eulerian formulation for creeping flows and applications in tectonic models, *Geophys. J. Int., 120*, 1-23, 1995.

Graf, H.R., Die Deckenschotter der zentralen Nordschweiz, Ph.D. thesis, 151 pp., Eidg. Techn. Hochsch., Zürich, Switzerland, 1993.

Guermani, A., and G. Pennacchioni, Brittle precursors of plastic deformation in a granite. An example from the Mont Blanc massif (Helvetic, Western Alps), *J. Struct. Geol., 20*, 135-148, 1998.

Handy, M R., L. Franz, F. Heller, B. Janott, and R. Zurbriggen, Multistage accretion and exhumation of continental crust (Ivrea crustal section, Italy and Switzerland), *Tectonics, 18*, 1154-1177, 1999.

Herwegh, M., O.A. Pfiffner, and K. Kunze, Dynamic recrystallisation of carbonate mylonites at the brittle-plastic transition: Evidence from the Helvetic Nappes paper presented at Deformation Mechanisms, Rheology and Microstructures Conference, GeoForschungsZentrum Potsdam and Justus-Liebig-Universität Giessen, Neustadt, Germany, March 1999.

Hynes, A., J. Arkani-Hamed, and G. Reinhard, Subduction of continental margins and the uplift of high-pressure metamorphic rocks, *Earth Planet. Sci. Lett., 40*, 13-25, 1996.

Jäckli, H., Der rezente Abtrag der Alpen im Spiegel der Vorlandsedimentation, *Eclogae. Geol. Helv. 51*(2), 354-365, 1958.

Jaoul, O., J. Tullis, and A. Kronenberg, The effect of varying water contents on the creep behavior of Heavitree quartzite, *J. Geophys. Res., 89*, 4298-4312, 1984.

Laubscher, H.P., The late Alpine (Periadriatic) intrusions and the Insubric Line, *Mem. Soc. Geol. Ital., 26*, 21-30, 1983.

Mancktelow, N.S., Neogene lateral extension during convergence in the Central Alps: Evidence from interrelated faulting and backfolding around the Simplonpass (Switzerland), *Tectonophysics, 215*, 295-317, 1992.

Milnes, A.G., Structure of the Pennine zone (Central Alps): A new working hypothesis, *Bull. Geol. Soc. Am., 85*, 1727-1732, 1974.

Nievergelt, P., and M. Liniger, Early to mid-Tertiary crustal extension in the Central Alps: The Turba Mylonite Zone (eastern Switzerland), *Tectonics, 15*, 329-340, 1996.

Niño, F., J. Chéry, and J.P. Gratier, Mechanical modeling of compressional basins; origin and interaction of faults, erosion, and subsidence in the Ventura Basin, California, *Tectonics, 17*, 955-972, 1998.

Okaya, N., S. Cloetingh, and S. Mueller, A lithospheric cross-section through the Swiss Alps; I, Thermokinematic modelling of the Neoalpine orogeny, *Geophys. J. Int., 125*, 504-518, 1996.

Ord, A , and B.E. Hobbs, The strength of the continental crust, detachment zones and the development of plastic instabilites, *Tectonophysics, 158*, 269-289, 1989.

Paterson, M.S., Problems in the extrapolation of laboratory rheological data, *Tectonophysics, 133*, 33-43, 1987.

Pfiffner, O.A., Alpine orogeny, in *A Continent Revealed: The European Geotraverse*, edited by D. Blundell, R. Freeman and S. Mueller, pp. 180-190, Cambridge Univ. Press. New York, 1992.

Pfiffner, O.A., and P. Heitzmann, Geologic interpretation of the seismic profiles of the Central Traverse (lines C1, C2, C3-north), in *Deep Structure of the Swiss Alps: Results of NRP 20*, edited by O A. Pfiffner et al., pp. 115-122, Birkhauser, Boston, Cambridge, Mass., 1997.

Pfiffner, O.A., P. Heitzmann, P. Lehner, W. Frei, A. Pugin, and M. Felber, Incision and backfilling of Alpine valleys. Pliocene, Pleistocene and Holocene processes, in *Deep Structrue of the Swiss Alps: Results of NRP 20*, edited by O.A. Pfiffner et al., pp. 265-288, Birkhäuser, Boston, Cambridge, Mass., 1997.

Pfiffner, O.A., and L. Hitz, Geologic interpretation of the seismic profiles of the Eastern Traverse (lines E1 – E3, E7 – E9). Eastern Swiss Alps, in *Deep Structrue of the Swiss Alps: Results of NRP 20*, edited by O.A. Pfiffner et al., pp. 73-100, Birkhäuser, Boston, Cambridge, Mass., 1997.

Pfiffner, O.A., E.M Klaper, A.-M. Mayerat, and P. Heitzmann, Structure of the basement-cover contact in the Swiss Alps, in *Deep Structure of the Alps*, edited by F. Roure, P. Heitzmann, and R. Polino, *Mem. Soc. Geol. Fr., 156*, 247-262, 1990.

Platt, J.P., Dynamics of orogenic wedges and the uplift of high-pressure metamorphic rocks, *Bull. Geol. Soc. Am., 97*, 1037-1053, 1986.

Ramsay, J G., *Folding and Fracturing of Rocks.*, 568 pp., McGraw-Hill, 1967

Ranalli, G., and D.C. Murphy, Rheological stratification of the lithosphere, *Tectonophysics, 132*, 281-295, 1987.

Rosenberg, C., A. Berger, and S.M. Schmid, Observations from the floor of a granitoid pluton: A constraint on the driving force of final emplacement, *Geology, 23*, 443-446, 1995.

Schlunegger, F., and S. Willett, Spatial and temporal variations in exhumation of the central Swiss Alps and implications for denudation mechanisms, in *Exhumation Processes: Normal Faulting, Ductile Flow and Erosion*, edited by U. Ring et al., *Geol. Soc. Spec. Publ., 154*, 157-179, 1999.

Schmid, S.M., What does nature tell us about rock rheology? Paper presented at Conference on Deformation Mechanisms, Rheology and Microstructures,

GeoForschungsZentrum Potsdam, Germany, 1999.

Schmid S.M., H.R. Aebli, F Heller, and A Zingg, The role of the Periadriatic line in the tectonic evolution of the Alps, in *Alpine Tectonics*, edited by M.P Coward, D. Dietrich, and R.G. Park, *Geol. Soc. Spec Publ., 45*, 253-171, 1989.

Schmid, S.M., O.A. Pfiffner, N. Froitzheim, G Schönborn, and E. Kissling, Geophysical-geological transect and tectonic evolution of the Swiss-Italian Alps, *Tectonics, 15*, 1036-1064, 1996

Schmid, S M., O.A. Pfiffner, G Schönborn, N. Froitzheim, and E. Kissling, Integrated cross section and tectonic evolution of the Alps along the Eastern Traverse, in *Deep Structure of the Swiss Alps: Results of NRP 20,* edited by O.A. Pfiffner et al , pp. 289-304, Birkhäuser, Boston, Cambridge, Mass , 1997b.

Schmid, S.M., O.A. Pfiffner, and G. Schreurs, Rifting and collision in the Penninic zone of eastern Switzerland, in *Deep Structure of the Swiss Alps: Results of NRP 20,* edited by O.A. Pfiffner et al., pp. 160-185, Birkhauser, Boston, Cambridge, Mass., 1997a.

Schmid, S.M , A Zingg, and M Handy, The kinematics of movements along the Insubric Line and the emplacement of the Ivrea Zone, *Tectonophysics, 135*, 47-66, 1987.

Schönborn, G., Alpine Tectonics and kinematic models of the central Southern Alps, *Mem Sci.Geol , XLIV*, 229-393, 1992

Shelton, G , and J. Tullis, Experimental flow laws for crustal rocks (abstract), *Eos Trans. AGU, 62*, 396, 1981.

Shemenda, A.I., and A Grocholsky, Physical modelling of lithosphere subduction in collision zones, *Tectonophysics, 216*, 273-290, 1992.

Stampfli, G.M., and R.H. Marchant, Geodynamic evolution of the Tethyan margins of the Western Alps, in *Deep Structure of the Swiss Alps: Results of NRP 20*, edited by O.A. Pfiffner et al., pp 223-240, Birkhäuser, Boston, Cambridge, Mass., 1997

Stampfli, G.M., J. Moser, D. Marquer, R. Marchant, T. Baudin, and G. Borel, Subduction and obduction processes in the Swiss Alps, *Tectonophysics, 296*, 159-204, 1998,

van den Beukel, J , Some thermomechanical aspects of the subduction of continental lithosphere, *Tectonics, 11*, 316-329, 1992.

von Blankenburg, F., H. Kagami, A. Deutsch, F. Oberli, M. Meier, M. Wiedenbeck, S Barth, and H. Fischer, The origin of Alpine plutons along the Periadriatic Lineament, *Schweiz. Mineral. Petrogr Mitt , 78*, 55-66, 1998.

Waldhauser F., E. Kissling, J. Ansorge, and S Mueller, Three-dimensional interface modelling with two-dimensional seismic data: The Alpine crust-mantle boundary, *Geophys J. Int., 135*, 264-278, 1998

Willett, S.D., Rheological dependence of extension in wedge models of convergent orogens, *Tectonophysics, 305*, 419-435, 1999.

Willett, S., C. Beaumont, and P. Fullsack, A mechanical model for the tectonics of doubly vergent compressional orogens, *Geology, 21*, 371-374, 1993.

Ye, S. Crustal structure beneath the central Swiss Alps derived from seismic refraction data, Ph.D thesis, 125 pp , Eidg. Techn Hochsch., Zürich, Switzerland, 1992.

C. Beaumont, Oceanography Department, Dalhousie University, Halifax, N.S. Canada B3H4J1

S. Ellis, Institute of Geological and Nuclear Sciences, Gracefield Rd, PO Box 30-368, Lower Hutt, New Zealand

O A Pfiffner, Geologisches Institut, Universität Bern, Baltzerstrasse 1, CH-3012 Bern, Switzerland

(Received November 16, 1999;
revised May 22, 2000;
accepted June 30, 2000.)